Earth and Space Science

RESEARCH ARTICLE
10.1029/2025EA004984

Characterizing Aerosol Modes and Uncertainty in VIIRS Aerosol Optical Depth Retrievals Over Africa Using AERONET

Shima Bahramvash-Shams[1], Robert C. Levy[2], Rajesh Kumar[1], Helen Worden[1], and Pieternel F. Levelt[1,3,4]

[1]National Center for Atmospheric Research, Boulder, CO, USA, [2]NASA-Goddard Space Flight Center (GSFC), Greenbelt, MD, USA, [3]Royal Netherlands Meteorological Institute (KNMI), De Bilt, The Netherlands, [4]University of Delft Technology, Delft, The Netherlands

Abstract Accurate characterization of aerosol optical depth (AOD) uncertainties is critical for air quality assessment, data assimilation (DA), and environmental studies. In this study, we evaluate two sets of AOD products retrieved from Suomi-NPP VIIRS over Africa. Specifically, we compare the products of NASA's Dark Target (DT) and Deep Blue (DB) algorithms with co-located AERONET observations from 2020 to 2024 over Africa. AERONET visible–near-IR Angstrom Exponents (AE) shows a bimodal distribution and strong monthly variability, with fine-mode dominance in August–September and coarse-mode dominance in March–April in this region. When the VIIRS retrievals are collocated with AERONET over Africa, DB shows a slight overestimation with DT showing a slight underestimation. When examined by AOD value range, DB shows a low bias under heavier aerosol loading, whereas DT exhibits a wider data spread and a less pronounced low bias at higher AOD values. Overall, DB demonstrates a higher correlation and a smaller expected error (EE) envelope compared to DT. Analysis of monthly uncertainty indicates that fine-mode-dominated months, particularly August, September, and October, which also contain the largest number of moderate to heavy aerosol loading cases, exhibit the lowest uncertainty in the DB retrievals, highlighting the improved performance of the updated algorithm. Our analysis shows that, for both DT and DB, AOD retrieval uncertainties are related to the observed AE, suggesting mismatches between algorithm assumptions and the actual dominant aerosol mode, particularly for coarse and mixed-mode aerosols.

Key Points:

- Angstrom Exponents exhibit strong monthly variability, indicating fine-mode dominance in September and coarse-mode dominance in April across Africa
- Validation of VIIRS SNPP using AERONET data shows the Deep Blue algorithm has lower uncertainties compared to Dark Target over Africa
- Uncertainties in satellite AOD retrievals are related to the dominant aerosol mode, via the proxy of Angstrom Exponent over Africa

Supporting Information:

Supporting Information may be found in the online version of this article.

Correspondence to:

S. Bahramvash-Shams,
sshams@ucar.edu

Citation:

Bahramvash-Shams, S., Levy, R. C., Kumar, R., Worden, H., & Levelt, P. F. (2026). Characterizing aerosol modes and uncertainty in VIIRS aerosol optical depth retrievals over Africa using AERONET. *Earth and Space Science*, *13*, e2025EA004984. https://doi.org/10.1029/2025EA004984

Received 7 JAN 2026
Accepted 20 APR 2026

Author Contributions:

Conceptualization: Shima Bahramvash-Shams
Formal analysis: Shima Bahramvash-Shams
Funding acquisition: Rajesh Kumar, Helen Worden, Pieternel F. Levelt
Investigation: Shima Bahramvash-Shams, Robert C. Levy
Methodology: Shima Bahramvash-Shams, Robert C. Levy
Validation: Shima Bahramvash-Shams
Visualization: Shima Bahramvash-Shams

1. Introduction

Aerosol particles in the atmosphere originate from a variety of sources including natural sources such as deserts, biomass burning, volcanoes, and oceans along with diverse anthropogenic sources (Boichu et al., 2019; Ginoux et al., 2012; Streets et al., 2003). Once airborne, the aerosol optical, physical, and chemical characteristics also evolve and change over time due to different physical and chemical processes during their transport and dispersion (Kleinman et al., 2020; Yu et al., 2013). Atmospheric aerosols particles are harmful to human health (Alexeeff et al., 2020; Burnett et al., 2018) and play an important role in Earth's radiative balance, cloud formation and lifetime, with large uncertainties in their effects on Earth's climate forcing (Liu et al., 2019; Rosenfeld et al., 2014), as well as hydrological systems (Kabir et al., 2018; Koren et al., 2012; Ramanathan et al., 2001). They have also been shown to contribute to cross-continental nutrient transfer with an important role in biogeochemical cycles (Barkley et al., 2019; Yu et al., 2015). Therefore, characterizing aerosol particle sources and properties is essential for understanding their impact on these different components of the earth system.

Africa experiences persistently high values of surface-level aerosol concentrations (e.g., particulate matter), intensifying over the past two decades (Xu et al., 2023). The rapid pace of urbanization across Africa, coupled with inadequate infrastructure and limited regulatory capacity, exacerbates the population's exposure to air pollution, posing substantial public health risks (Hill et al., 2014). Africa is shown to be a significant source of global biomass-burning, especially during the dry season (Ichoku & Ellison, 2014; van der Werf et al., 2017). Also, half of the world's mineral dust aerosols originate from Africa (Ginoux et al., 2004). Convective updrafts can carry African dust emissions high into the atmosphere, where they undergo long-range transport due to altitude-dependent differences in dry and wet removal (Ridley et al., 2012). It is estimated that more than 200 Tg of dust from Africa is annually deposited downwind, including into the Atlantic (Ridley et al., 2012).

Writing – original draft: Shima Bahramvash-Shams, Robert C. Levy, Rajesh Kumar, Helen Worden, Pieternel F. Levelt
Writing – review & editing: Shima Bahramvash-Shams, Robert C. Levy, Rajesh Kumar, Helen Worden, Pieternel F. Levelt

Generally, aerosols from combustion-related processes like transportation, industry and biomass burning tend to be of a smaller (finer) size (e.g., equivalent radius) than aerosols arising from mechanical processes like wind-driven emissions of dust or sea salt. Observations of aerosol size distribution (frequency as a function of radius) often show two or more approximately lognormal modes which include a "fine" mode and a "coarse" mode. Since Africa has so many sources of fine-mode and coarse-mode aerosols which mix during transport, relative dominance of one mode or the other helps indicate the aerosol type. Also, aerosol sources and meteorology/transport processes vary by season. The separation of particles is defined as where particles with radii smaller than 0.6 μm are considered as fine, with particles with radii larger than 0.6 μm as coarse mode (Dubovik et al., 2002). Ambient aerosols may include both fine and coarse -sized aerosols, but often one size mode is often dominant.

Monitoring surface-level particulate matter in Africa is expensive and challenging, however globally polar-orbiting satellite sensors are being used to monitor and quantify the total-column aerosol optical properties. In particular, remote observations from sensors such as Moderate Resolution Imaging Spectroradiometer (MODIS), the Multiangle Imaging SpectroRadiometer (MISR), and Visible Infrared Imaging Radiometer Suite (VIIRS), provide spatial and temporal coverage of aerosol information, including the AOD and spectral dependence of the AOD known as AE, across the globe (Huang et al., 2016; Kahn et al., 2010; Kaufman et al., 1997; Remer et al., 2005). These retrievals are useful for many applications, such as monitoring aerosol loads (Bahramvash-Shams & Mohammadzadeh, 2015) and the assimilation of satellite-borne aerosol data for air-quality forecasts (Kumar et al., 2020; Liu et al., 2011) and weather forecasts (Huang et al., 2023; Kumar et al., 2020; Morcrette et al., 2009). Although MODIS and MISR retrievals and data sets have long been a "standard" for global aerosol properties including over Africa, their satellite platforms (Terra and Aqua) have been orbiting for more than two decades and will be decommissioned soon. MISR has already been turned off, with Terra and Aqua slowly drifting out of orbit since 2021 and 2022, respectively. The MODIS operations will likely end 2026–2027 (NASA-Aqua, 2025; NASA-Terra, 2025). To mitigate loss of the aerosol data record, two of the MODIS aerosol retrieval algorithms (Dark Target and Deep Blue) have been ported to be used on VIIRS family of sensors, beginning with the VIIRS on the Suomi-National Polar-orbiting Partnership (SNPP) satellite platform. Preliminary validation studies of VIIRS on S-NPP reported overall consistency with MODIS at the global scale, while also identifying notable regional and surface-dependent biases in VIIRS AOD retrievals (Huang et al., 2016; Liu et al., 2014). Given that surface albedo and aerosol type vary substantially across regions and directly influence AOD retrieval accuracy, regional characterization of errors and uncertainties is necessary (Shi et al., 2013). Comparative studies over East Asia, India, the Mediterranean, and the Amazon highlight pronounced regional differences in AOD product performance versus global estimates (Ettehadi Osgouei et al., 2022; Meng et al., 2015; Payra et al., 2023; Schumacher & Setzer, 2024; Zhu et al., 2017). While globally focused studies have shown VIIRS uncertainties over Africa, such as underestimates of AOD during the agricultural burning season (Huang et al., 2016), and NOAA-20 VIIRS AOD underestimation in Southern Africa (Pei et al., 2025), to our knowledge, no study has conducted a detailed uncertainty quantification of NASA SNPP VIIRS AOD over Africa.

Detailed quantification of uncertainties in any data set, including satellite data, allows all users, scientific and applied, to better understand the capabilities and limitations of the data and to interpret the results accordingly. Moreover, a detailed estimate of uncertainties of satellite AOD products and EE are needed to properly constrain air quality forecasting systems using data assimilation methods. Uncertainties in satellite retrievals arise from many sources, not limited to radiative-transfer model error, retrieval parameterizations, surface-reflectance estimation, aerosol optical assumptions, and reliance on look-up tables (Kaufman et al., 1997). Since aerosols over Africa are diverse, and there is a limited database of *in situ* aerosol and land surface optical information, it is unknown whether satellite aerosol retrievals in the region have similar or larger uncertainties than other regions which are observationally dense. Since the assumption of aerosol type impacts the AOD retrieval accuracy, it is important to fully understand the characteristics of aerosols in the region.

Here we evaluate the uncertainty for both DB and DT retrievals, the monthly variations of uncertainties, as well as the potential pattern due to assumptions of aerosol size. Since AE is a proxy for relative aerosol size, we use this metric that is directly measured by the Aerosol Robotic Network (AERONET; Holben et al., 1998). Therefore, an objective of this paper is to characterize AE distributions and the seasonal variability of potential dominant aerosol modes, using AERONET data across Africa.

To better understand the uncertainties of retrieval algorithms, first we investigate the characteristics of aerosols using AERONET data and the seasonality of aerosols characteristics in the region. Then, this paper characterizes the uncertainty of 550 nm AOD from VIIRS on SNPP, for both Deep Blue and Dark Target algorithm over Africa and provides quantification of biases and the EE, which is critical for data assimilation applications over the region. We focus on AOD products over lands and use recent years, 2020 to 2024, to provide an updated EE. This uncertainty estimation is suited for incorporation in air quality forecasting systems via chemical data assimilation systems, is based on co-located AERONET ground measurements and VIIRS retrievals. This approach is similar to past validation methodology of different satellite aerosol products (Huang et al., 2016; Kahn et al., 2010; Levy et al., 2018; Remer el al., 2005). The structure of the paper is as follows. Section 2 introduces the data sets used in this study. Section 3 explains the methodology for analysis, pair creation, and evaluation. Section 4 describes the characterization of aerosol modes over Africa, and Section 5 focuses on the evaluation of all VIIRS AOD against AERONET data for each algorithm. Section 6 discusses the seasonal characteristics of biases and error variances. Section 7 examines VIIRS uncertainties based on aerosol modes. Section 8 provides further discussion of the results and lessons learned.

2. Data

2.1. VIIRS

The first VIIRS sensor was launched aboard the SNPP satellite in 2011. Although similar in many ways to MODIS, it has wider swath widths that avoids gaps in its coverage (Huang et al., 2016). VIIRS retrieves AOD using multiple spectral bands spanning 412–2,250 nm; the exact band set depends on the algorithm (Hsu et al., 2019; Jackson et al., 2013; Sawyer et al., 2020, 2025). NASA has ported two of its MODIS-heritage algorithms for retrieving aerosols over land from VIIRS SNPP. The Dark Target (DT) algorithm targets vegetated, dark surfaces (Sawyer et al., 2020) whereas the Deep Blue (DB) includes retrievals over brighter (e.g., desert) surfaces and later to more surface types (Hsu et al., 2013, 2019). Note that both products are considered "Level 2" (L2) products, which means that their products are reported along the orbit track, rather than gridded to a standard spatial resolution. Both algorithms provide multi-wavelength AOD at a nominal (nadir viewing) 6 km spatial resolution. Retrievals of AOD are paired with a quality control flag that represents expected confidence assigned during the retrieval, enabling data filtering. Both algorithms provide AOD at 550 nm.

DT and DB algorithms have undergone independent upgrades and processing history. Here we use Version 2.0 (V2) for each product, in which both represent upgrades from their initial versions. In case of DT (Levy et al., 2024; Sawyer et al., 2025; and LAADS User Doc), in addition to updated, calibrated inputs (known as Level 1B), V2 introduced higher-resolution cloud masking, higher-resolution meteorological reanalyzes as ancillary data, an alternate sediment mask near coastal regions, and an alternate equation for estimating surface "greenness". Many of these DT updates were intended to improve continuity with DT on other sensors (e.g., MODIS), so overall impacts were intended to be minimal. For DB (Lee et al., 2024; and LAADS User Doc), the overall upgrades were more significant, including updates for land surface elevation, a new surface reflectance database, new aerosol models, and smoke detection schemes. Note that V2 for DB includes a "calibration factor" that generally reduces AOD globally, whereas DT did not introduce such a factor until the next version (V2.1). DT V2.1 was not yet available for this analysis.

Products of the DT and DB algorithms are denoted as AERDT_L2_VIIRS_SNPP and AERDB_L2_VIIRS_SNPP respectively, and are publicly available at NASA's Level-2 and Atmosphere Archive and Distribution System (LAADS) Distributed Active Archive Center (DAAC) at https://ladsweb.modaps.eosdis.nasa.gov/.

Both DT and DB algorithms lead to multiple variables representing AOD over land and ocean separately, and then combined according to Quality Assurance (QA). Here, we analyze the QA-controlled AOD variables known as "Aerosol_Optical_Thickness_550_Land_Best_Estimate" (for DB) and "Optical_Depth_Land_And_Ocean" (for DT). Both of these variables represent AOD in the green wavelength (550 nm). While both these variables are intended as being QA-controlled, the DT over-land AOD had not been filtered correctly for inclusion into the combined Land_And_Ocean variable. Therefore, we refiltered, according to the recommended QA thresholds (e.g.., QA $\geq$ 2 over land), ensuring that only moderate to higher confidence AOD retrievals are used in our analysis. Although the DT product was corrected for their Version 2.1, it was not available at time of this analysis.

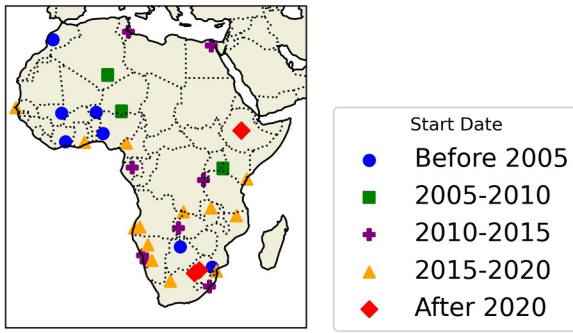

Figure 1. Location and start date of active AERONET stations over Africa. This map includes the sites that have valid measurements from January 2020 to December 2024. The start date of sites is categorized into 5 groups, before 2005 up to after 2020.

Finally, it should be noted that although both DT and DB report AOD on a 6 km resolution box, there is no requirement that both retrieve for the same box. Due to requirements of scene brightness (vegetation vs. deserts), spatial homogeneity and other thresholds being met or failed during retrieval, there are cases for both, one or the other, or neither algorithm retrieving AOD. In general, DB has a much greater coverage over all (vegetation and bright surfaces), with DT avoiding the bright surfaces but applied to pixels closer to identified clouds.

2.2. AERONET

AERONET is a global, collaborative network of ground-based remote sensing stations that use sun-photometers to measure aerosol optical properties (Giles et al., 2019; Holben et al., 1998). The data collected at these sites provide detailed information on vertical aerosol loading, size distribution, and type, serving as a critical reference for validation of satellite-based aerosol retrievals (Huang et al., 2016; Kahn et al., 2010; Levy et al., 2013–2018; Remer et al., 2005) as well as trend analysis (Zhang et al., 2025). Depending on the site, time-of-day and measurement type protocols, AERONET data are provided at different temporal resolutions (Giles et al., 2019), and are publicly available at https://aeronet.gsfc.nasa.gov/. Specifically, the "direct-sun" measurements of spectral (multi-wavelength) AOD are provided at 5–15 min intervals. We use AERONET AE at 440–870 nm for size distribution analysis. To be comparable to VIIRS AOD, we estimated AOD at 550 nm by fitting a second-order polynomial to ln (AOD) as a function of ln (wavelength), using AOD at 440, 500, and 675 nm, following the spectral formulation of Eck et al. (1999), which are expected to be accurate within 0.01 (Eck et al., 1999; Schuster et al., 2006). AERONET data includes multiple levels of processing, such that Level 1.5 data are data that are collected and reported immediately, and Level 2 requires post-reprocessing that includes laboratory re-calibration, extra cloud-screening, and application of temperature corrections (Giles et al., 2019). Depending on the site's accessibility and maintenance schedule, it may take months or years for data to be upgraded from Level 1.5 to Level 2. Although Level 1.5 data may be more numerous, here we use the Level 2 to ensure the highest level of quality control, which is essential for error characterization of satellite AOD retrievals.

AERONET spatial coverage is sparse over Africa, and most of the sites have been added only recently. Figure 1 maps the locations of AERONET stations that were active at some time between January 2020 to December 2024, and categorizes their era of first deployment. The start date of sites is categorized into 5 groups, before 2005 up to after 2020. Although spatial coverage gaps remain large, particularly over central Africa, by 2020 the spatial representation of AERONET sites across East, South, and North Africa has improved. It should be noted that many sites in the 2015–2020 category were installed during the last two years of this period. Therefore, while the VIIRS–SNPP data record began in 2011, we focus on the 2020–2024 period, and use Level 2 data to ensure adequate spatial coverage across the continent.

Table 1 introduces the 35 AERONET sites that were active and provided Level 2 data during at least part of this study. Table 1 also includes the time range of available Level 2 data, and information about the statistics of the data and the number of collocations with both DT and DB data sets from VIIRS-SNPP between January 2020 to the end of December 2024. Note that some sites did not report during the entirety of 2020–2024. Ethiopia only recently (2022) added a site (site name: AAU_Jackros_ET). At other sites, the Level 2 data period ends early—either they have stopped reporting, or the Level 2 data has not yet been created. Some sites are pairwise compatible with DT and not DB or vice-versa (primarily due to whether being a desert site or not). Although AOD data from a few stations did not qualify for pair-wise validation at all, we use these sites for our aerosol-characterization analysis. For instance, AERONET data from Dakar_Belair, Senegal is located on a coastline of the Atlantic Ocean, such that there are not enough "over-land" VIIRS aerosol retrievals within the required distance criteria (e.g., 27.5 km radius around the site) to be included in the validation. However, its long data record helps to characterize the aerosol properties as discussed in Section 4. A detailed criteria description is provided in Section 3.

Table 1
Statistics of Valid Data and Characterization of AERONET Sites, in Alphabetical Order

	Station	Latitude	Longitude	Processed Lev 2 period		Valid AERONET data	NDB	NDT
1	AAU_ET	9.019	38.748	2020–01	2022–10	9,555	55	65
2	AAU_Jackros_ET	9.012	38.821	2022–10	2025–03	24,812	80	199
3	ASI_Malindi	−2.996	40.194	2018–04	2025–03	36,043	271	413
4	Banizoumbou	13.541	2.665	1995–10	2025–02	19,621	69	2
5	Bujumbura	−3.380	29.384	2013–12	2024–10	220	NA	10
6	Cairo_EMA_2	30.081	31.290	2010–04	2025–03	24,865	44	70
7	CATUC_Bamenda	5.949	10.156	2016–12	2024–12	7,904	50	57
8	Dakar_Belair	14.702	−17.426	2019–05	2025–03	45,577	NA	NA
9	Durban_UKZN	−29.817	30.944	2013–05	2023–12	18,765	122	156
10	Gobabeb	−23.562	15.041	2014–11	2024–10	60,529	733	NA
11	Henties_Bay	−22.095	14.260	2011–11	2024–05	253	1	2
12	HESS	−23.273	16.503	2016–02	2025–03	83,006	728	487
13	ICIPE-Mbita	−0.417	34.200	2006–03	2025–03	25,590	7	186
14	IER_Cinzana	13.278	−5.934	2004–06	2025–03	26,689	26	10
15	Ilorin	8.320	4.340	1998–04	2025–03	34,528	117	174
16	Koforidua_ANUC	6.109	−0.302	2015–12	2025–03	7,863	13	40
17	LAMTO-STATION	6.224	−5.027	1997–06	2025–03	17,324	3	11
18	Lubango	−14.958	13.445	2016–02	2024–11	7,232	154	160
19	Maun_Tower	−19.900	23.550	2000–09	2025–03	37,784	316	437
20	Medenine-IRA	33.500	10.643	2014–07	2025–03	26,629	21	NA
21	Metsi	−26.491	27.132	2020–10	2025–02	46,765	293	279
22	Misamfu	−10.171	31.224	2015–01	2025–03	34,107	202	334
23	Mongu_Inn	−15.267	23.134	2013–09	2025–03	38,877	254	409
24	Namibe	−15.159	12.178	2016–02	2023–10	5,972	58	11
25	Niassa	−12.155	37.567	2019–06	2024–10	1,126	20	46
26	Pretoria_CSIR-EC	−25.750	28.278	2020–05	2025–03	25,184	263	322
27	Saada	31.626	−8.156	2004–07	2024–04	4,962	1	1
28	Sakeji_School	−11.233	24.312	2017–08	2024–09	1,875	76	103
29	SEGC_Lope_Gabon	−0.202	11.601	2014–04	2025–03	6,827	NA	53
30	Skukuza	−24.992	s31.588	1,998–07	2025–03	40,584	467	556
31	Tamanrasset_INM	22.790	5.530	2006–09	2025–03	37,255	221	NA
32	UEM_Maputo	−25.950	32.599	2019–06	2025–03	3,473	85	208
33	Upington	−28.379	21.156	2016–02	2025–03	57,146	481	125
34	Windpoort	−19.366	15.483	2016–02	2025–03	48,502	505	542
35	Zinder_Airport	13.777	8.990	2009–05	2025–03	7,658	38	6

Note. A valid AERONET data point is one where AERONET observes in at least at three wavelengths as required for estimating AOD at 550 nm, from January 2020 to end of December 2024. NDB and NDT are the numbers of paired data with respect to VIIRS DB and DT AOD 550 nm.

3. Methodology

3.1. AE as Proxy for Aerosol Size Distribution

Aerosol optical depth is commonly reported and compared at a 550 nm wavelength, which represents the optical aerosol loading near the peak of the solar spectrum. Measuring the exact size distribution of aerosol particles by

remote sensing is an extremely challenging task. The spectral dependence of the AOD across the solar spectrum is related to the relative aerosol size, however AERONET does not generally measure across the entire spectrum. Therefore, we use AE as a metric to inform on aerosol size distribution, defined as below (Eck et al., 1999):

$$\mathrm{AE} = -\frac{\ln\left(\frac{\tau_a}{\tau_b}\right)}{\ln\frac{\lambda_a}{\lambda_b}}$$

Where τ_a and τ_b represent AOD at two wavelengths, λ_a and λ_b represent the corresponding wavelengths, respectively. Here, we used the standard AERONET AE product, defined over the wavelength range 440–870 nm, to investigate the aerosol size distribution characteristics in the region and potential influence of aerosol size distribution on VIIRS uncertainties.

The relationship between AE and particle size distribution is not linear. In general, AE values closer to 0 indicate dominance of coarse-mode aerosols including dust and sea-salt, while values approaching 2 indicate fine-mode aerosols emitted by biomass burning and anthropogenic sources, and values around 1 likely indicate a mix of aerosol types (Eck et al., 1999). Previous studies have used AE thresholds, multi-index thresholds, and clustering approaches to provide more detailed aerosol classification (Bilal et al., 2022; Eck et al., 1999, 2010; Giles et al., 2012; Mishra et al., 2025 and reference within) where each approach has limitations when classifying aerosols with complex mixtures and overlapping characteristics. Here, since we are looking for an overall understanding of regional and seasonal algorithm performance, we focus on distribution analysis and have chosen to use $\mathrm{AE} = 1$ to separate aerosol regimes. Although $\mathrm{AE} \approx 1$ may indicate mixed aerosol types, the bi-modal distribution AE in this regional and seasonal scale is supported by histograms. We also examine the full distributions using histograms and box plots to better characterize distribution shifts, variations in peak values, and potential dominant modes when present.

Since the uncertainty of AERONET AE is larger for lower load of aerosol (Sayer, 2020), we require that AOD 550 nm is greater than 0.2 for size distribution analysis to ensure the robustness of the analysis (Sayer, 2020). The analysis of aerosol characteristics is conducted by using all AERONET data with $\mathrm{AOD} > 0.2$, during the full 5 years to better understand the properties of aerosols in the region.

3.2. VIIRS AOD Validation

As excluding AOD 550 nm smaller than 0.2 would dramatically reduce the number of VIIRS-AERONET collocated pairs, the analysis of VIIRS AOD uncertainties is conducted by using all the paired data, which also allows quantification of uncertainties in low AOD values. Differences in spatial and temporal sampling can affect the comparison, because satellite AOD represents a spatial average while AERONET provides point measurements that may not coincide with the satellite overpass time. This potential mismatch, together with the spatial/temporal thresholds used to create satellite–AERONET pairs, can influence the sampling and uncertainty estimates (Martins et al., 2017; Mishra et al., 2023). Here, to create the pairs for comparisons, AERONET data within ±30 min of VIIRS overpass at each station and VIIRS pixels in radius of 27.5 km around each station are collected and averaged, according to the protocol suggested by Petrenko et al. (2012) and has also been used for VIIRS validation studies (Huang et al., 2016; Pei et al., 2025). We applied quality control thresholds to the collocations including: retrieval quality flag ≥2 for both DB and DT VIIRS data, a minimum of 9 high quality VIIRS retrieval pixels within the 27.5 km radius, and at least 4 AERONET data points must be available in a 1-hr window. A few stations provide negligible comparable data to VIIRS, since they did not meet the co-located pair-creation criteria for DT or DB or both. Note that due to choices made by each retrieval algorithm, some collocations will represent only one of the two retrieval products as shown in Table 1.

The correlation analysis directly investigates the AOD, hereafter assumed to be at 550 nm, from VIIRS (retrieved) versus AERONET (interpolated). We analyze the AOD bias, defined as AERONET AOD minus VIIRS AOD, as a function of VIIRS AOD. This prognostic error analysis enables implementation in the DA framework, where only satellite AOD is available to define the uncertainties.

To investigate the correlations, we first applied the Shapiro test to assess the normality of the paired data distributions. As $p < 0.05$ indicated non-normality, the nonparametric Spearman correlation coefficient was used instead of the Pearson correlation coefficient. To characterize the estimated error (EE), VIIRS AOD data are

clustered into 0.1 AOD bins and for each bin the standard deviation (STD) and mean bias is estimated and a fitted line on STDs is used to define the error estimate envelope. The STD of each bin is included in estimating the fitted line if at least 3 data points existed in that bin.

To account for the limited and variable number of matched AERONET and VIIRS observations available in each month, we applied a Monte Carlo resampling approach to derive robust estimates of the regression parameters. For each month, we repeatedly sampled 50%, 70%, and 90% of the available data without replacement across 100 iterations. In each iteration, a linear regression was fitted to the sampled data, and the slope, intercept, and nonparametric Spearman correlation coefficient were recorded. For the final reported Spearman correlation coefficient, the mean ± standard deviation of all iterations is used and for the regression the mean of slope and intercept is used. For the monthly EE, the same binning method used for all data is applied to each month, and the mean of slope and intercept are calculated across iterations and checked to satisfy the 67% confidence interval to satisfy the error envelope. Monte Carlo resampling helps to reduce sensitivity to outliers or small-sample anomalies and enhances the statistical robustness of the monthly analysis by incorporating uncertainty due to sample variability.

The pairing code and all the statistical analyses are available at Bahramvash-Shams (2026).

4. Characterization of Aerosol Modes

Knowing the size distribution of aerosols helps to identify their sources and quantify their radiative forcing. In this study, we assume that the AE threshold of 1 separates fine- from coarse-dominated aerosol cases, and that AOD >0.2 indicates a sufficient aerosol loading for making that distinction. In Section 7 we investigate whether the identified grouping of AE (potentially indicating dominant fine, coarse modes) impacts the accuracy of satellite retrievals.

Figure 2 shows the histogram of AE, separated monthly, aggregated over all African AERONET stations between 2020 and 2024. This analysis is limited to AOD > 0.2 to ensure confidence in AE, the result exhibited a large monthly variability of moderate to enhanced aerosol loadings. September has more than 50,000 AE values, which is 40% more than 2nd place August, and 170% more than November with the fewest. For better illustration of histogram AOD for each month is shown in Appendix A. Figure S1 in Supporting Information S1, which shows a decreasing frequency by increasing AOD load for all month.

For relative frequency of AE, there is also a large variability from month to month. February through June exhibit a higher frequency of AE < 1, with the highest occurrence below 0.3 in March and April, supporting strong dominance of coarse particles. In contrast, August and September show predominantly AE > 1, with histogram peaks above 1.7 indicating strong dominance of fine-mode particles. November shows AE approximately 1 indicating mixed aerosol (neither fine nor coarse-dominated). In October there are nearly equal frequencies of low AE and high AE values, which may indicate variability from day-to-day. For simplicity, we denote months with higher fraction of low AE values as "coarse," those with higher fraction of high AE values as "fine," and those that are nearly equal or have a large fraction of AE near 1 as "mixed." When there are more data values that fraction is more robust.

To further illustrate the monthly variability, continent-wide monthly AE data are shown as a box-whiskers-plot in Figure 3. March to May skew toward low AE values, with April and May showing medians around 0.4 and a narrow spread, indicating dominance of coarse-mode aerosols. In contrast, August and September exhibit much higher AE, with medians above 1.6 and similarly narrow distributions, indicating dominance of fine particles. July and October have the largest spread of AE values. While July and November both have AE medians close to 1, July has a large variability suggesting all types of aerosols, whereas November with its smaller variability suggests more cases of "mixed" aerosols. Starting in October, AE peak median values decrease, reaching a minimum in April, when aerosols are dominated by coarse particles. Another conclusion is that during November (with the least number of observations, e.g., fewer cases of medium and heavy aerosol loadings) and during July there is no real dominance by fine or coarse modes.

The dominance of fine-mode aerosols in August and September is likely associated with biomass burning events as significant change in anthropogenic emission is not expected for these months and large biomass burning during these months is confirmed through burned area and emission analysis over Africa (Tatro & Zuidema, 2025). The peak CO signal observed by MOPITT in September 2004 and the minimum burned area

10.1029/2025EA004984

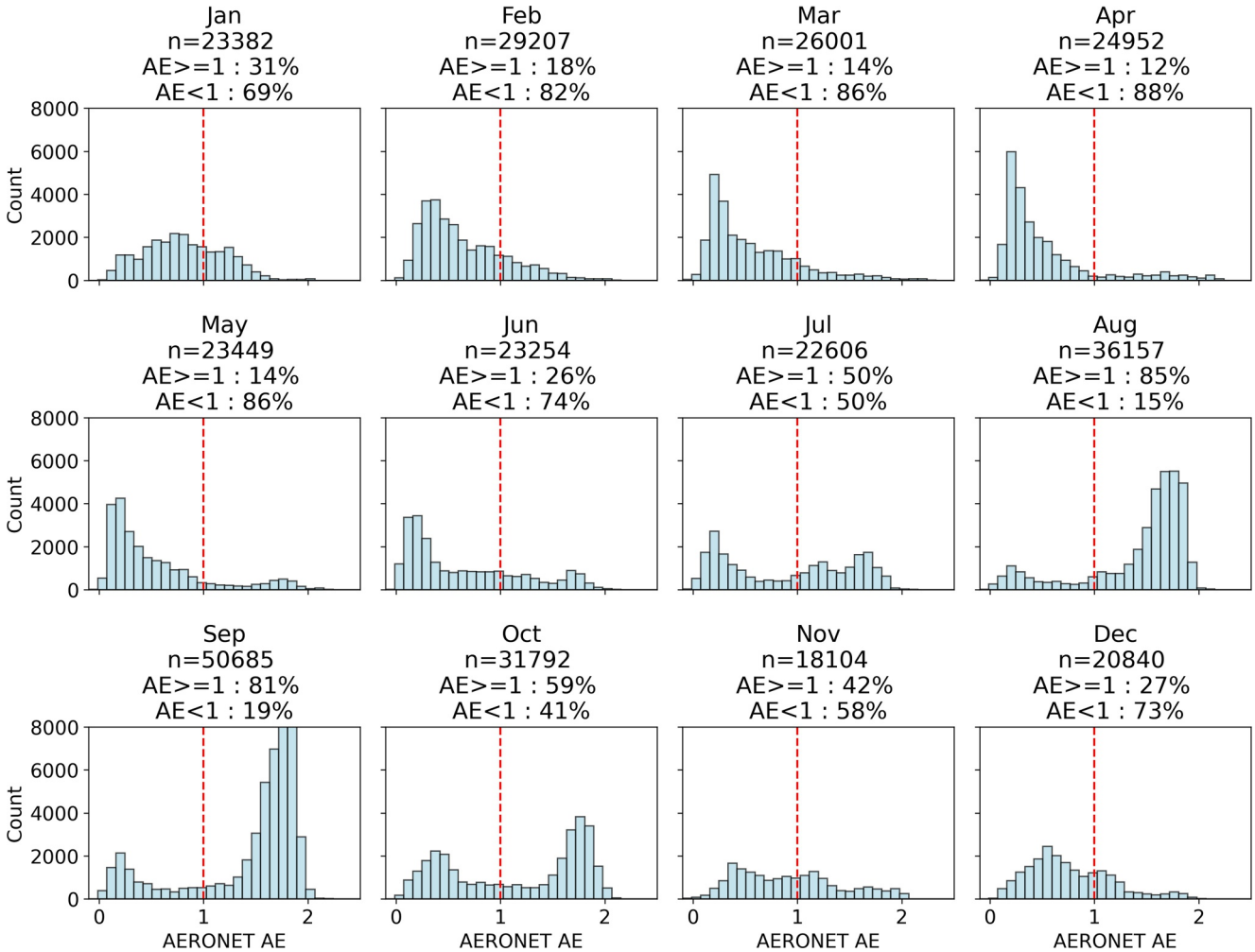

Figure 2. The histogram of AE across all African AERONET stations over Africa for each month, by criteria of AOD > 0.2, which represents moderate to high aerosol load. The red dashed line shows the AE equal to 1. The total number of high-quality AE for each month and percentage of AE >= 1 and AE < 1 particles are shown on top of each subplot.

observed in Africa during April and May 2004 from previous studies are consistent with our results (Roberts et al., 2009).

To understand the geospatial characteristics of aerosol modes across the continent, Figure 4a shows the AERONET sites based on their dominant aerosol mode. Figure 4 also incorporates the histogram of AE data for stations grouped by the dominant aerosol modes: coarse, fine, and mixed, which are plotted in overlapping histograms on subplots. Stations are assigned a dominant aerosol type if more than 80% of their AE data points satisfy the threshold of AE > 1 or AE < 1 for AOD > 0.2, as explained in the methodology section, and otherwise it is labeled "mixed" to reflect either a nearly equal contribution of low AE and high AE or a dominant AE near 1. The marker size in Figure 4a reflects the number of valid AERONET observations from 2020 to 2024 for each site that were incorporated into the aerosol mode analysis. Figures 4b–4d show homogeneity of sites in each aerosol mode group as indicated by the clean overlap of AE histograms for stations. The dominance of coarse mode aerosol particles (blue dots) in north Africa is consistent with proximity to the dust belt over north Africa. The only blue dot in the east, ASI_Malindi at Kenya, has been shown to be mostly impacted by sea-salts aerosols from the Indian Ocean/Arabian Sea and local dust aerosols (Boiyo et al., 2019). All AERONET sites in southern Africa and some in Central Africa are dominated by fine particles, which have significant biomass burning episodes and burned fraction (van der Werf et al., 2017) in addition to anthropogenic sources.

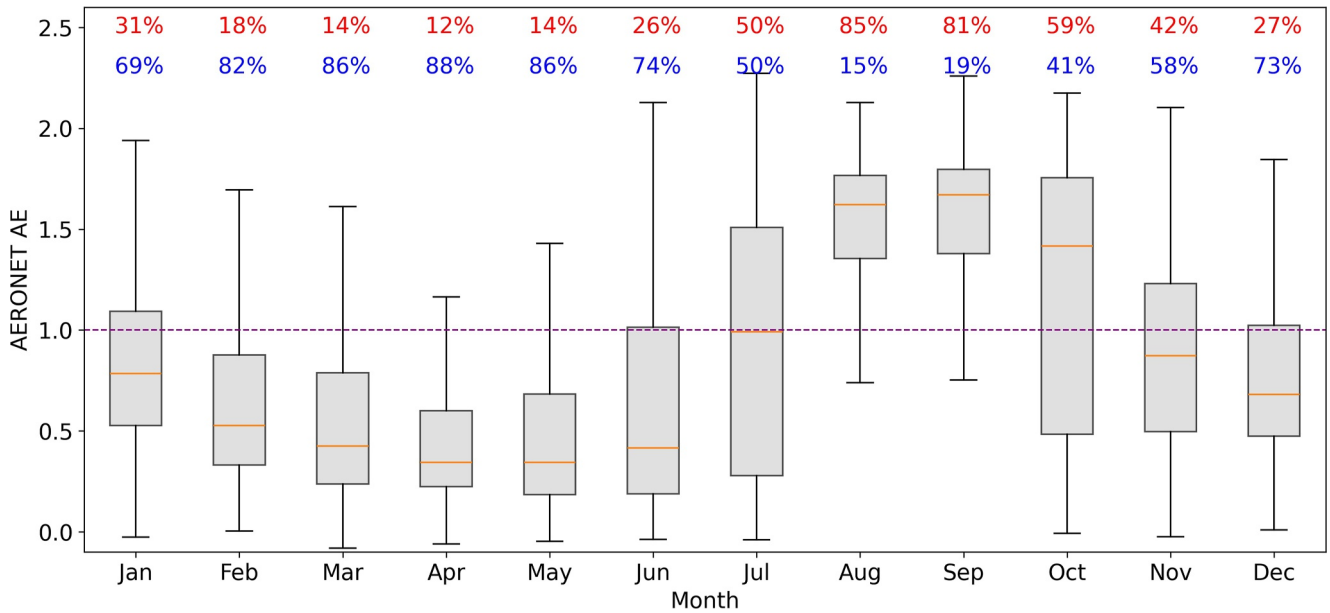

Figure 3. The aggregated signal of AE across all AERONET stations over Africa by month. The red and blue color % show the percentage of fine and coarse mode particles respectively. The horizontal dashed purple line indicates the AE equal 1, the median value of AE is shown by the orange line, the 25th percentile and 75th percentile are shown as the limit of the box-whiskers.

The histograms for the red stations (Figure 4d) indicate that nearly all AE values exceed 1 and peak higher than 1.5, while an opposite pattern is observed for the blue stations, with AE values predominantly below 1 and peak below than 0.5. When interpreted in the context of the seasonal aggregation shown in Figures 3 and 4, these patterns point to lower aerosol loading during the March–April period for the red stations and during August–September for the blue stations. Some AERONET sites in Central Africa also exhibit a mixed aerosol mode, predominantly in the northern regions and along the coastal areas. Other AERONET inversion products provide additional parameters, such as particle linear depolarization ratio and fine-mode fraction (Mishra et al., 2025), in future studies this data can be used to enhance discrimination between aerosol populations and reduce mixed cases.

5. Evaluation of VIIRS Versus AERONET

Here we evaluate the accuracy of the satellite aerosol retrievals, using all paired data including low AOD <0.2. As noted in Table 1, due to the sampling and specifications of each retrieval algorithm as well as cloud treatments, there are different numbers of paired VIIRS/AERONET collocations for DT and DB. In addition, because a "pair" represents both multiple VIIRS retrievals (within the 27.5 km radius) and AERONET measurements (within the one-hour window). We include the statistics of paired data for this case study and data sets to provide transparency on the basis of the subsequent analysis.

In the ideal case, representing high-confidence quality, near-nadir viewing (smaller surface area per pixel), and a completely cloud-free scene over a suitable land surface, although we set a minimum of 9 retrievals for a valid collocation, there can be up to 78 VIIRS observations within the 27.5 km radius. At the same time, although we required at least 4 AOD measurements for an AERONET instrument within an hour, there are sites, time periods, and conditions for which there may be significantly more. Figure 5 plots histograms (overall and seasonal) for the number of valid observations in paired data. Interestingly, although the regional and AERONET-site specific DT and DB collocations are very different the overall number of collocations (5,474 vs. 5,774) for four years over all of Africa are similar.

Even though an ideal case (near-nadir, cloud-free, surface-artifact-free) is up to 78 VIIRS retrievals per collocation, this value is rarely attained for the often-cloudy scenes, heterogenous surfaces over Africa. Therefore, the number of high-confidence AOD retrievals is often lower, mainly between 15 and 48 pixels for DT and 40 to 60 for DB. These differences are rooted in details of the algorithm from land cover specification of retrieval

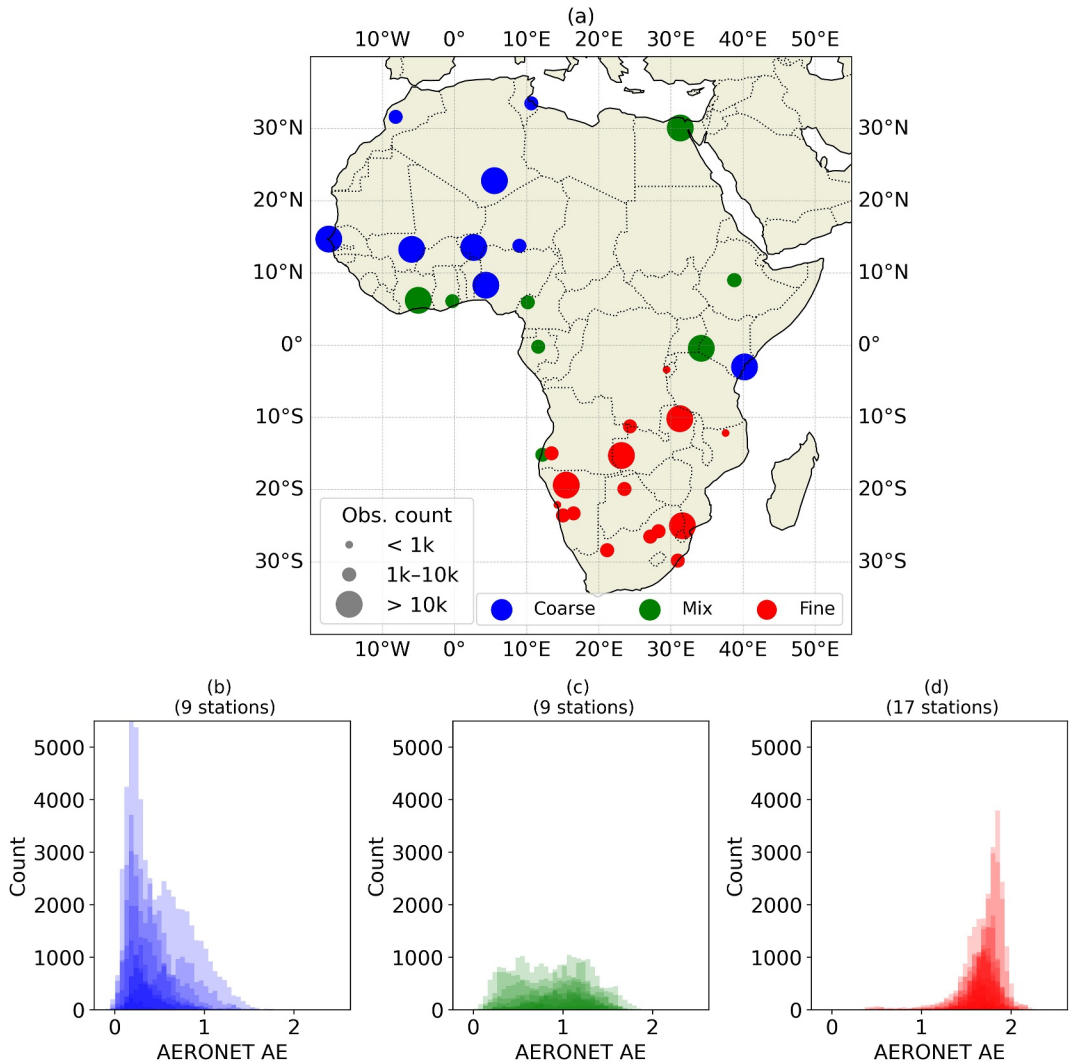

Figure 4. Spatial characterization of AERONET stations by the dominant aerosol mode (a), along with the histogram of all AE data associated with stations grouped by each dominated aerosol mode: coarse (b), mixed (c), and fine (d). The number of stations in each aerosol mode grouping is shown above the bottom row of plots. The number of valid AERONET observations with AOD > 0.2 at each station is also represented using three categories, fewer than 1k, between 1k and 10k, and greater than 10k, indicated by marker size in panel (a). The histograms are plotted with high transparency (alpha = 0.2) to highlight overlapping distributions.

algorithm, such as expansion of DB to non-bright surfaces as well as differences in treatment of cloud contaminations in these algorithms (Hsu et al., 2013, 2019; Sawyer et al., 2020). AERONET paired data are dominated by 10 measurements in the 1-hr window as shown in Figure 5. While most AERONET sensors report AOD at a 5-min temporal frequency, a few sensors provide data with a 3-min update frequency in some periods, which explains some occurrences of AERONET measurements higher than 12 in Figure 5, such as for Pretoria_CSIR-EC (25.8°S, 28.3°E), South Africa, in 2023.

Figures 5c and 5d also illustrates the seasonal distribution of the number of VIIRS pixels used to create collocated pairs for both algorithms. The highest frequency of larger numbers of VIIRS pixels occurs during June, July, and August, satisfying the criteria for both algorithms, as indicated by the red lines in Figures 5c and 5d. In contrast, during the austral summer (December, January, and February) exhibit the highest frequency of lower numbers of VIIRS pixels meeting the criteria, as shown by the blue lines in Figure 5. This reduction is likely driven by increased cloud cover during the wet season, as documented for southern Africa (Hart et al., 2013).

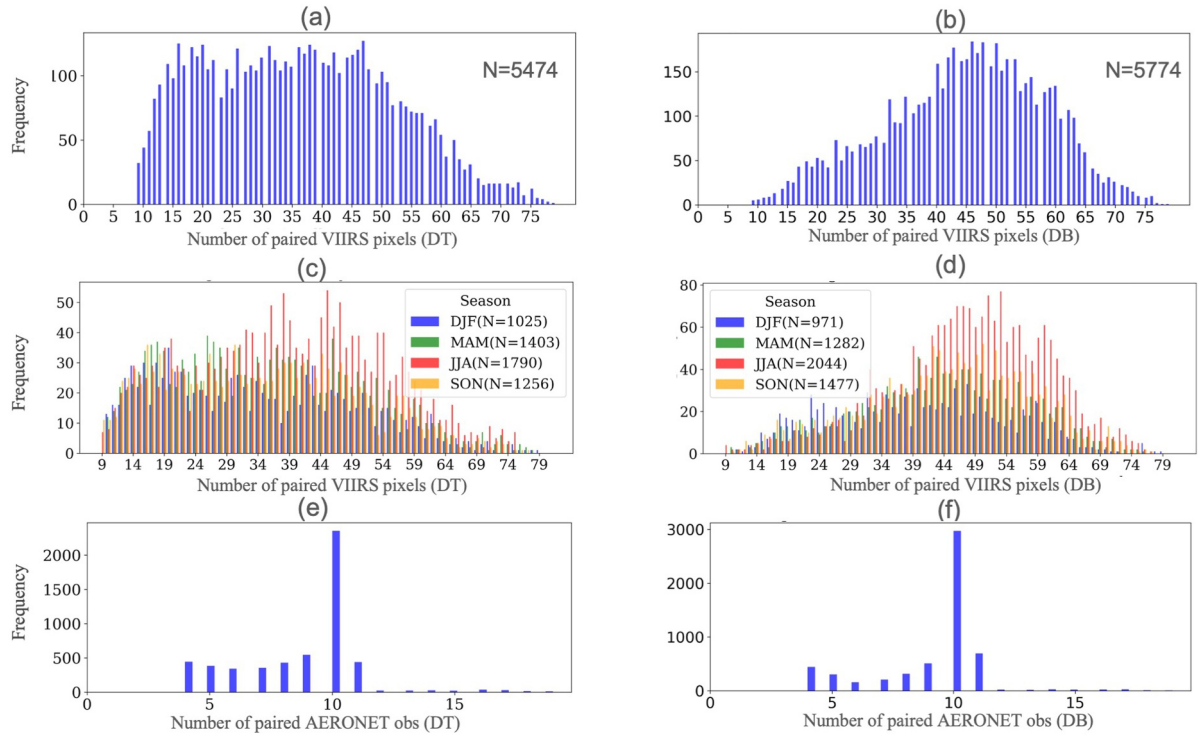

Figure 5. Statistics of the number of observations that are averaged in the included pairs in the analysis, (a, e) show the histogram of VIIRS and AERONET for DT pairs in the analysis, respectively. (b, f) show the histogram of VIIRS and AERONET for DB pairs in the analysis. The seasonal representation of VIIRS in the co-located pairs for DT and DB are shown in panels (c, d), respectively.

The statistics of paired AOD for both DT and DB are shown in Figure 6, where the upper row shows distribution of VIIRS AOD and the lower row shows distribution of AERONET minus VIIRS AOD, respectively. VIIRS AOD in the pairs shows skewed histogram peaks at AOD values between 0.05 and 0.2, with samples covering the full range of AOD up to around 1. There are limited VIIRS paired data between AOD values of 1 and 2, with very

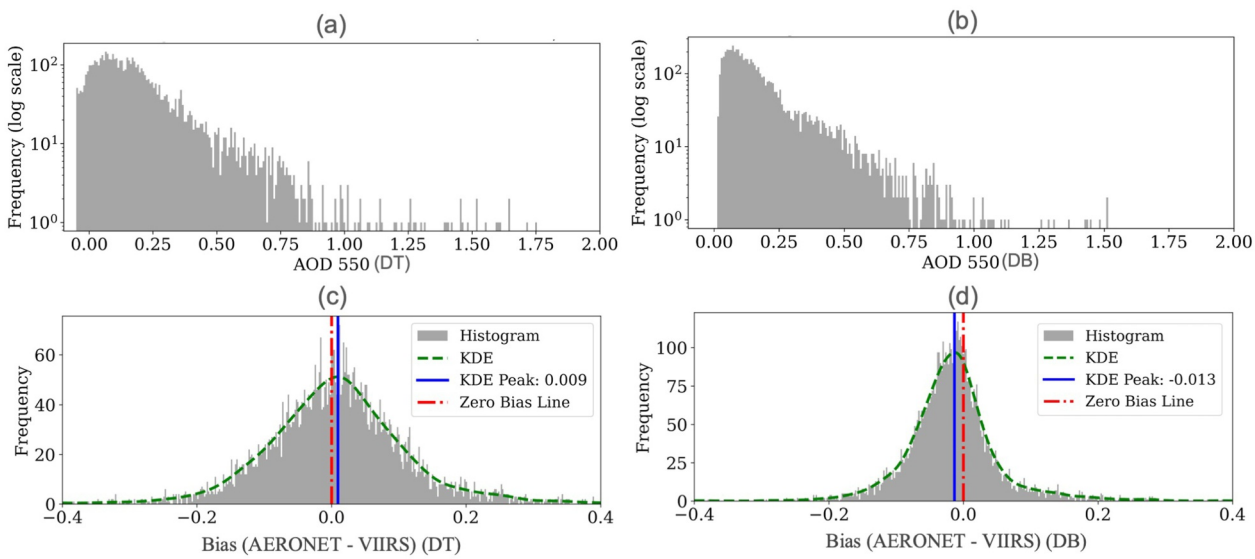

Figure 6. Statistics of AOD and bias for paired sets. Panels (a, c) show histograms of VIIRS AOD and bias (AERONET minus VIIRS) for DT pairs, respectively; panels (b, d) show the corresponding histograms for DB pairs. The red dashed dot line is the zero line, solid blue line shows the highest frequency peak value, and the dashed green line indicates the fitted KDE line.

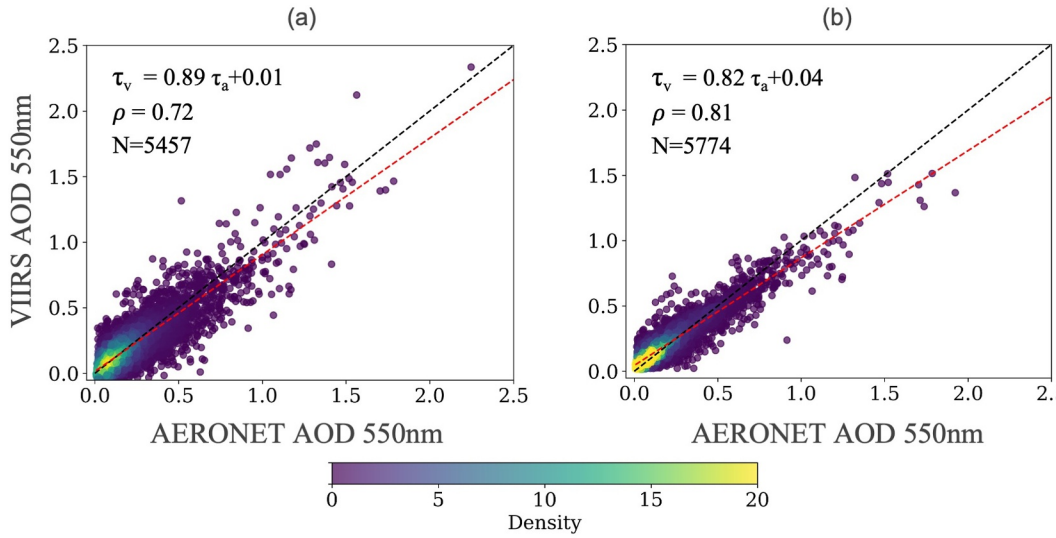

Figure 7. The density plot between AERONET and VIIRS AOD at 550 nm for (a) DT and (b) DB algorithm. Black dash lines show the one-to-one line and the red dash line shows the fitted line on the data. The fitted equation, Spearman correlation coeffienct, and total number of data is shown for each subplot. VIIRS AOD is shown by τ_v and AERONET AOD is shown by τ_a in the fitted equations.

few pairs showing AOD values higher than 2 in the case of DT. To maintain readability, the *x*-axis of both subplots (a) and (b) in Figure 6 is truncated at an AOD of 2. It should be noted that a small negative AOD of −0.05 in DT, subplots (a) Figure 6, is influenced by the bias correction of DT data production methodology (Levy et al., 2024).

Figure 6 also shows the biases between paired data, AERONET minus VIIRS, which nearly exhibit a Gaussian distribution in both DT and DB. We applied kernel density estimation (KSE) as a non-parametric method to fit a smooth probability distribution over the histogram of bias values. The peak of the KDE curve was then used to estimate the most frequent observed bias. VIIRS DT exhibits underestimation with a magnitude bias of 0.009. DB on the other hand shows slight overestimation, the magnitude bias of 0.013 as the peak value of its distribution and it has a narrower distribution in comparison to biases of VIIRS DT algorithm, Figure 6d.

The correlation between VIIRS and AERONET AOD are shown in Figure 7. The Spearman correlation coefficient is higher for DB with ρ of 81% in contrast to 72% for DT. The regression line shows a larger drift for DB as AOD increases, and overall, for AOD larger than 1, VIIRS DB has a low bias. The spread of DT scatters against AERONET is larger which causes the fit line to be slightly closer to one-to-one line and not a visible pattern of bias at high AOD is observed. Figure 8 Showed the EE estimation for the VIIRS AOD for both DT and DB, as a function of VIIRS AOD. As expected, the uncertainties of VIIRS get magnified by increased AOD, for both algorithms, however the uncertainty of DT exhibit larger magnitudes as indicated by $EE = 0.11\tau_v + 0.09$ in contrast to the $EE = 0.07\tau_v + 0.07$ for DB, where τ_v is VIIRS AOD, for both DB and DT. The more consistent performance of DB is likly related to recent algorithm updates, including accounting for surface pressure, enhanced characterization of surface reflectance, and the addition of a new fine-mode aerosol optimal model (Lee et al., 2024). On the other hand, the aerosol models used in DT (Levy et al., 2007) were developed using the limited AERONET observations available during 1993–2005, which included only a handful from Africa (e.g., Figure 1). Incorporating updated aerosol models that represent more detailed optical and physical characteristics could further improve the performance of retrieval products (Mishra et al., 2025).

6. Seasonal Characteristics of Biases and Error Variances

Both DT and DB algorithms show overall good skill with moderate and higher levels of AOD. However, it is clear from Figure 8 that there are still biases. DT and DB algorithms assume aerosol models that are based on AERONET to some extent, and AERONET sampling over Africa is now significantly improved since these algorithms were developed. Our analysis in Section 4 reveals pronounced monthly variations in the dominant

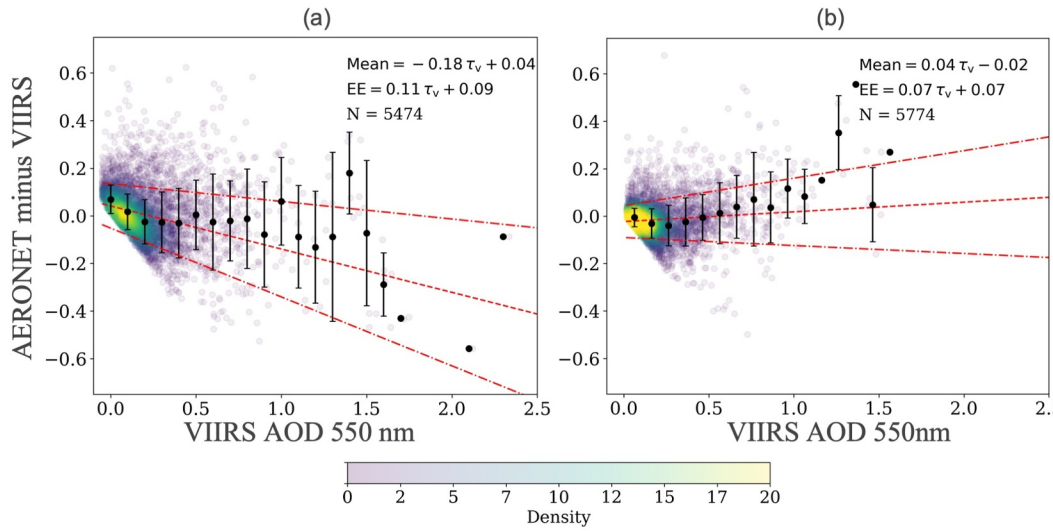

Figure 8. The density scatter plot of biases between AERONET and VIIRS AOD at 550 nm with respect to change in VIIRS AOD for (a) DT and (b) DB algorithm. Error bars show the std of each bin of 0.1 AOD and the red dash line shows the fit line to mean bias values at each bin and red dash dot line are fit of std values of biases at each bin added to the mean bias line to estimate EE. The fitted equations and total number of data is shown for each subplot. VIIRS AOD is shown by τ_v.

aerosol mode, as reflected in the variability of AERONET AE data and the shifting peaks of the AE histograms. Additionally, natural changes in land cover and surface reflectance are expected to contribute to variability in VIIRS performance and uncertainty quantification on a monthly basis. Therefore, we also performed a monthly validation, collecting the monthly paired data and using Monte Carlo sampling technique to minimize the impact of outliers in limited sample sizes. The statistics of monthly comparisons for both DT and DB pairs are shown in Table 2.

As a large part of Africa is in the tropical region, persistent cloudiness (e.g., during rainy seasons) significantly reduces the number of matched pairs and decreases the robustness of a statistic. The 5-month period from May to

Table 2
The Statistics of Monthly Comparisons for Both DT and DB Pairs Applied by Monte Carlo Analysis Which Includes Total Number of Pairs, the Regression Line, Spearman Correlation Coefficient and the EE

	DT				DB			
Month	N	τ_v=	ρ± error	EE=	N	τ_v=	ρ± error	EE=
Jan	357	$0.66\tau_a \pm 0.08$	0.76 ± 0.02	$0.03\tau_v \pm 0.13$	374	$0.73\tau_a \pm 0.05$	**0.83 ± 0.02**	$0.10\tau_v \pm 0.06$
Feb	337	$0.93\tau_a \pm 0.03$	0.73 ± 0.02	$0.05\tau_v \pm 0.13$	290	$0.87\tau_a \pm 0.03$	0.75 ± 0.03	$0.08\tau_v \pm 0.06$
Mar	354	$1.07\tau_a \pm 0.02$	0.73 ± 0.02	$0.20\tau_v \pm 0.05$	277	$0.76\tau_a \pm 0.05$	0.68 ± 0.03	$0.21\tau_v \pm 0.02$
Apr	406	$0.88\tau_a \pm 0.03$	0.73 ± 0.02	$0.37\tau_v \pm 0.01$	362	$0.83\tau_a \pm 0.04$	0.74 ± 0.02	$0.11\tau_v \pm 0.03$
May	**643**	$1.24\tau_a - 0.01$	0.62 ± 0.02	$0.11\tau_v \pm 0.03$	**643**	$0.91\tau_a \pm 0.04$	0.59 ± 0.02	$0.16\tau_v \pm 0.03$
Jun	**582**	$1.11\tau_a \pm 0.01$	0.58 ± 0.02	$0.06\tau_v \pm 0.04$	**692**	$0.90\tau_a \pm 0.04$	0.62 ± 0.02	$0.24\tau_v \pm 0.02$
Jul	**629**	$0.88\tau_a \pm 0.00$	0.59 ± 0.02	$0.07\tau_v \pm 0.06$	**654**	$0.93\tau_a \pm 0.03$	0.81 ± 0.01	$0.17\tau_v \pm 0.02$
Aug	**579**	$0.77\tau_a \pm 0.00$	0.77 ± 0.01	$0.08\tau_v \pm 0.08$	**698**	$0.79\tau_a \pm 0.04$	**0.89 ± 0.01**	$0.04\tau_v \pm 0.06$
Sep	**529**	$0.95\tau_a - 0.02$	**0.84 ± 0.01**	$0.07\tau_v \pm 0.08$	**681**	$0.89\tau_a \pm 0.05$	**0.91 ± 0.01**	$0.03\tau_v \pm 0.06$
Oct	388	$1.07\tau_a - 0.02$	0.77 ± 0.02	$0.05\tau_v \pm 0.08$	463	$0.85\tau_a \pm 0.04$	**0.87 ± 0.01**	$0.04\tau_v \pm 0.06$
Nov	339	$0.80\tau_a \pm 0.03$	0.63 ± 0.03	$0.12\tau_v \pm 0.06$	333	$0.73\tau_a \pm 0.04$	0.68 ± 0.03	$0.30\tau_v \pm 0.02$
Dec	331	$0.75\tau_a \pm 0.04$	0.67 ± 0.03	$0.13\tau_v \pm 0.07$	307	$0.70\tau_a \pm 0.05$	0.72 ± 0.02	$0.06\tau_v \pm 0.06$

Note. The Spearman correlation is shown by mean ± std of all Monte Carlo sampling and shown as bold if higher than 80% and sample numbers higher than 500 are also depicted as bold. VIIRS AOD 550 nm is shown by τ_v and AERONET AOD 550 nm by τ_a. The lowest EE is highlighted by light gray for each methodology.

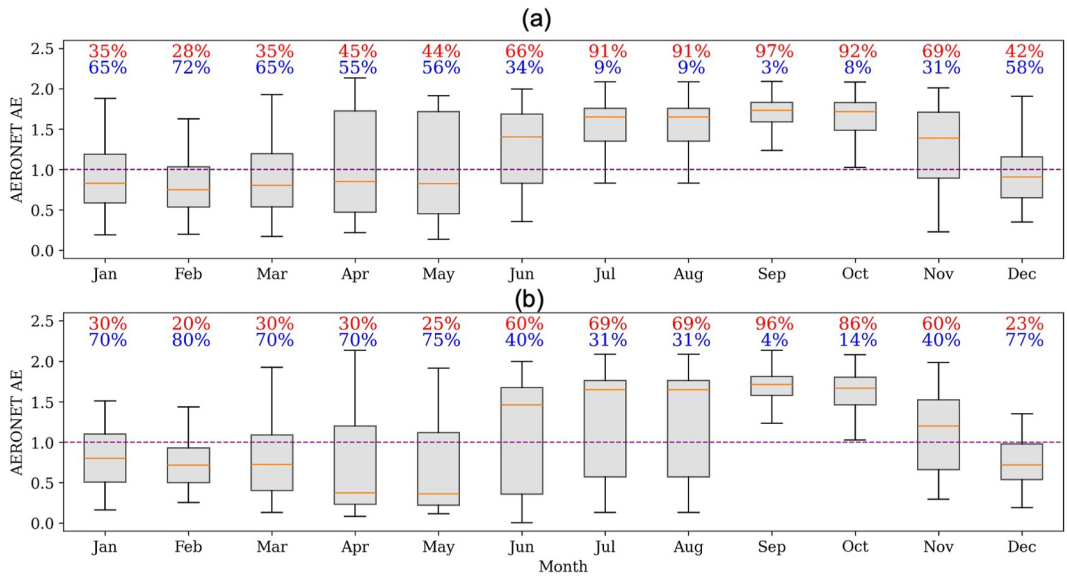

Figure 9. The aggregated AE AERONET data for co-located pairs with VIIRS over Africa by month (a) for DT algorithm and (b) for DB algorithm. The red and blue color % show the percentage of AE ≥ 1 and AE < 1 particles respectively. The horizontal dashed purple line indicates the AE equal 1, the median value of AE is shown by the orange line.

September exhibited the highest number of paired data in both algorithms with more than 600 cases for DB and 500 cases for DT as shown in Table 2. Compared to VIIRS DT, the VIIRS DB product showed a higher ρ with respect to AERONET for four of these months, with ρ higher than 80% with small variability ±0.02 at most (based on 300 rounds of Monte Carlo samplings). May, June, and November showed low correlation in both retrieval methodologies. Yet the VIIRS DB tends to overestimate at low aerosol loads (positive intercept), which aligns with Figure 3d histogram dominated by small AOD values. As AOD increases, the bias becomes increasingly negative, consistent with slopes below 1 across all months in table 2 for DB and with the slope observed in Figure 7b. DT exhibits more variability in its matching statistics, with 4 months showing high bias at elevated AOD (slope greater than 1) and month-to-month variability in the intercept's sign. August, September, and October showed the smallest EE envelope, which represents the covariance error estimate in AOD DA, with around $0.04\tau_v + 0.06$, while the lowest is September with $0.03\tau_v + 0.06$ for DB retrieval. During June and July, EE envelopes are the smallest for the DT algorithms, with $0.06\tau_v + 0.04$ and $0.07\tau_v + 0.06$. The covariance error (EE envelopes) was largest in March, June, and November for DB with $0.21\tau_v + 0.02$, $0.24\tau_v + 0.02$, and $0.30\tau_v + 0.02$: and highest in April and March for DT algorithm with $0.37\tau_v + 0.01$ and $0.20\tau_v + 0.05$. March and April show the strongest dominance of coarse-mode particles, as illustrated in Figures 2 and 3 for all AERONET data. During these months, DT exhibits its lowest performance, suggesting limitations in coarse-mode retrieval; this issue is discussed further in Section 7. Because the DT retrieval relies on a limited set of aerosol models representing a few fine- and only one coarse-mode types. In addition mixed-mode aerosol load may introduce additional uncertainty and contribute to higher EE in some months. Characterizing uncertainty and errors on a monthly basis can help inform air quality DA frameworks by incorporating monthly observation covariance errors and establishing realistic expectations for forecast performance. For example, our results indicate that DB shows the most consistent performance during August, September, and October, which coincide with periods dominated by fine-mode aerosols and enhanced biomass burning activity.

7. VIIRS Uncertainties Based on AE and Dominant Aerosols Mode

We also investigate if VIIRS biases and EE for each retrieval algorithm is influenced by AE as a potential indicator of dominant aerosol mode. Therefore, we focused on AOD higher than 0.2 to ensure the AE quality. The criteria required for creating high quality co-located pairs between AERONET and VIIRS significantly changes the number of samples and potentially could influence the distribution of aerosol modes that are sampled through matched pairs. To ensure that the distribution of aerosol modes in the paired data is consistent with all the aggregated AERONET data or analyzing potential differences, Figure 9 shows the box plot of AE from

AERONET data associated with the paired data for both algorithms. The percentages shown above each box in Figure 9 are based on AE ≥ 1 and AE < 1 and are included to track shifts in the distribution, while the box-and-whisker plots illustrate the full AE distribution for each month.

The general pattern of dominance of fine particles in September/August is evident for paired data of both algorithms. However, DT has captured a higher contribution of fine mode particles from all months if compared with all AERONET data (comparing Figure 9a again Figure 2). The highest difference in June and July that AERONET AE of paired DT data showed 40% higher contribution of fine mode in contrast to all AERONET data, with 66% and 91% against 26% and 50% (Figure 9b again Figure 2). However still September is the most fine-mode dominated, with a very small range of values.

Overall, the percent contribution of fine versus coarse mode is closer to all AERONET data for DB, with the highest differences in June and July at 34% and 19% (the fine mode fraction from DB paired AERONET minus all AERONET data), respectively for each month (Figures 2 and 9b). The monthly pattern of AE for DB captures the dominance of coarse particles in April and May similar to that seen in investigation of all AERONET data, Figures 2 and 9b. In particular, the median values (orange vertical lines in the box plots) are consistent in Figures 2 and 9b, showing AE lower than 0.5 for April and May, box-whiskers horizontal boundaries. However, the spread of the middle 50% of AE values is larger in DB paired data compared to all AERONET data for April and May. On the other hand, in August, DB paired AERONET collection was impacted by both aerosols more with 69% AE ≥1 versus 85% for all AERONET data. September constantly shows high percent contribution of fine aerosol modes in both algorithms with 97% and 96% for DT and DB, respectively and very narrow inter-quartile range (Figure 9), and 81% for all AERONET data (Figure 4_1). This means that limited existing coarse mode cases in this month are filtered out in co-located pair selection as well. Overall, the comparisons show that the general pattern of monthly variability in aerosol modes is captured in both paired DT and DB AERONET AE data sets. However, for months in which the dominance of one mode is not pronounced, as expected based on the retrieval algorithm design, AERONET from DT paired has captured more fine-mode particles, while DB has captured more coarse-mode particles.

This subsampling, filtering of AOD < 0.2, dramatically impacts the total number of pairs for this analysis, as it excludes about 76% and 69% of the data for DB and DT, respectively. The higher cutoff for DB paired data is consistent with the higher frequency of samples below 0.2, as shown in Figure 6. Figure 10 shows the scatter plot of VIIRS against AERONET AOD based on AE ≥ 1 and AE < 1 groupings for both algorithms. To illustrate the potential existence of dominant aerosol mode for these groups, AE histograms are shown in the right corner of each subplot in Figure 10. In both VIIRS algorithms, we have more samples in AE ≥ 1 grouping with 1,270 and 1,015 compared to 449 and 390 for AE < 1, respectively. For the AE ≥ 1 group, the histograms indicate that these samples are dominated by fine-mode aerosols, with peaks above 1.5. In contrast, the AE < 1 group reflects a mixture of mixed and potentially coarse aerosol modes without a clearly dominant mode. Consistent with other section analysis, DB has higher ρ and narrower spread around the regression line in both AE categories compared to DT. The Spearman correlation coefficient is higher at AE < 1 with 0.84 for DB, while a solid performance is exhibited for DB in AE ≥ 1 with $\rho = 0.80$ which also is dominated by fine-mode aerosols. The range of higher AOD values in AE < 1 extends up to AOD of 2 for both algorithms. DB exhibits the best correlation, $\rho = 0.84$, in AE < 1 among the four comparisons in Figure 10, while it also shows an evident pattern of underestimation in VIIRS AOD at high aerosol loads. DT for AE < 1, which is not exhibiting a particular dominate aerosols, shows the lowest ρ with 0.69 and highest spread of data, Figure 10c.

Figure 11 shows the density plot of biases against VIIRS AOD 550 nm with associated fitted EE envelope and mean value of errors for both algorithms and both AE groupings. The mean bias for bins, the dark circle middle of bars in Figure 11, has a nonlinear structure for AE < 1 which is potentially a combination of mix and coarse mode aerosols in both algorithms. In AE ≥ 1 grouping, with fine-mode dominant particles, errors increase with AOD. In contrast, in the AE < 1 the binned mean and standard deviation are strongly nonlinear. Among all 4 comparisons, DB in AE ≥ 1, has the lowest covariance error with $EE = 0.07\tau_v + 0.06$, particularly for AOD smaller than 1.5; as it is followed by DB in AE < 1 grouping with $EE = 0.06\tau_v + 0.08$. The more consistent performance of DB in the AE ≥ 1 group compared to AE < 1 suggests better performance for predominantly fine-mode aerosols, as supported by the AE histograms. Our results across Sections 6 and 7 support the conclusion that DB shows strong performance in retrieving AOD associated with fine-mode aerosols over Africa. In contrast, the AE < 1 group represents a mixture of coarse-mode and mixed aerosols. While mixed aerosol conditions can increase

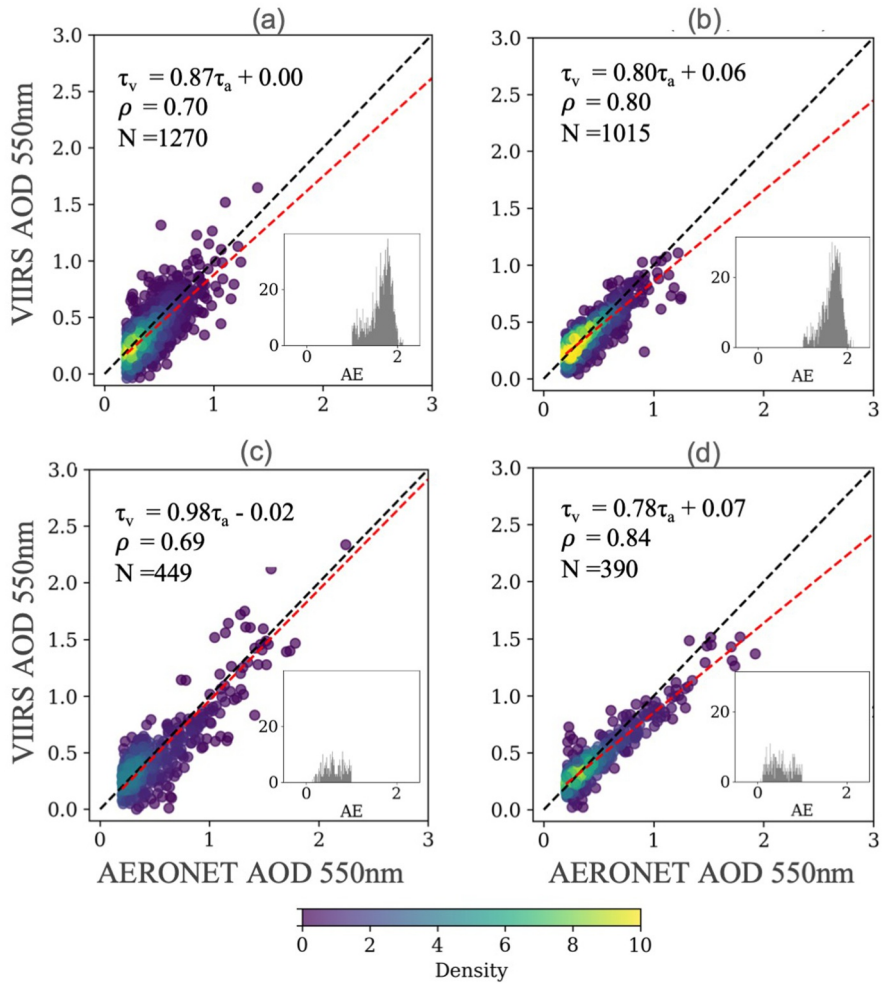

Figure 10. Scatter plot of AERONET versus DT VIIRS AOD 550 nm for AE ≥ 1 and AE < 1, is shown in panels (a, c) respectively. (b, d) similarly represent comparisons for the DB algorithm. The fit equation shows τ_v as VIIRS AOD 550 nm and τ_a as AERONET AOD 550 nm. The total number of samples in each group and Spearman correlation coefficient are also shown on each subplot. The histogram of AE for each subset of data is shown on the corner of each subplot.

uncertainties, another challenge lies in the simplified representation of coarse-mode aerosols in retrieval algorithms. These aerosols are typically described by a single optical model that does not capture the full variability of coarse particles. For example, recent studies have shown that carbon-coated dust particles can exhibit absorbing properties that are not represented in existing retrieval algorithms (Mishra et al., 2025). Incorporating more advanced aerosol models could improve retrieval performance across a wider range of aerosol modes and types.

8. Discussion and Conclusion

The main objective of this study is to quantify the uncertainties of NASA VIIRS land AOD products over Africa. To properly characterize the uncertainty of AOD retrievals, it is important to understand the relationship between retrieval assumptions versus the reality of the conditions being observed. One step is to determine the current characteristics and type of aerosols over the continent and how they vary monthly. By analyzing the AERONET AOD products, we can determine whether mismatches between retrieval assumptions and observed conditions contribute to AOD uncertainties.

Therefore, first we analyzed quality assured AERONET Level 2.0 measurements from 35 AERONET stations across Africa from January 2020 to December 2024. Using AE as a proxy, we have developed a modern climatology of fine-versus coarse-mode dominated aerosols over Africa. Analysis of AE distributions and peak locations shows that AERONET sites in North Africa are dominated by coarse-mode aerosols, displaying a

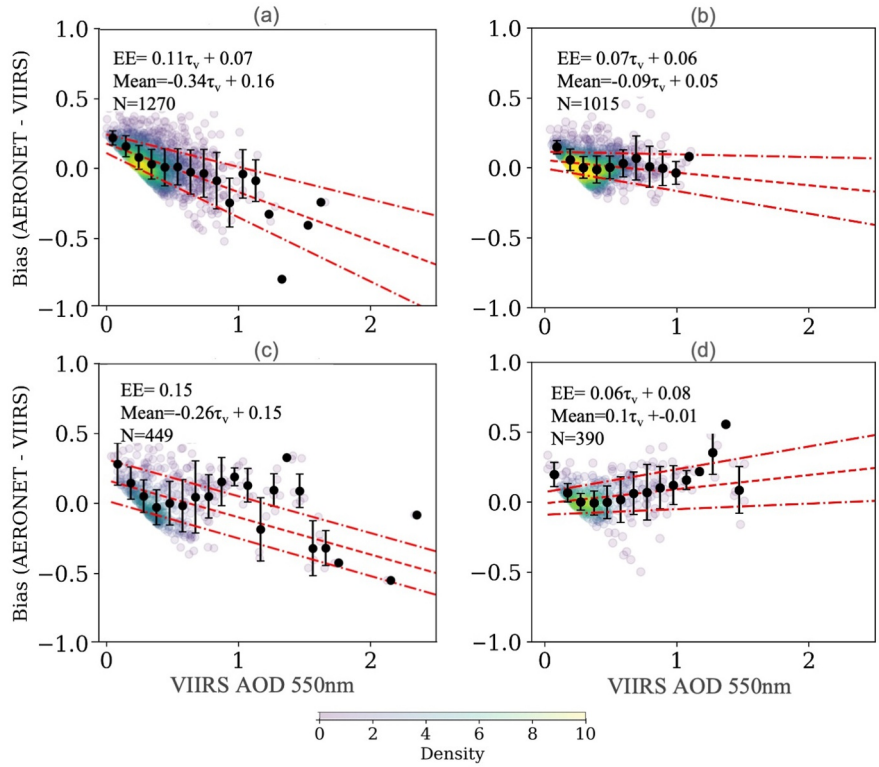

Figure 11. Scatter plots of biases against VIIRS AOD (550 nm) for AE grouping. Panels (a, c) depict DT data for AE ≥ 1 and AE < 1, respectively; panels (b, d) present the corresponding DB data. The final fit on the standard deviation, EE, indicates the covariance error. The total number of samples in each group is also shown on each subplot.

consistent geospatial pattern due to their proximity to the Saharan dust belt. Some sites in East Africa are influenced by sea-salt aerosols and local dust sources. In contrast, most sites in southern Africa and parts of Central Africa are dominated by fine particles associated with biomass burning and anthropogenic emissions, while several sites in northern and coastal Central Africa exhibit mixed aerosol conditions.

Our analysis showed wide variability of AE which suggests a strong monthly variability of aerosol mode. During April to May coarse mode particles are dominant, possibly linked to intense dust activities and August and September are dominated by fine mode particles due to intense biomass burning activities in addition to anthropogenic emissions in the region. September is the most contaminated month in terms of aerosol load, with the highest number of AE quality-assured data (more than 50,000 samples), corresponding to a high frequency of moderate to heavy aerosol loads, with a criterion of at least an AOD of higher than 0.2. Additionally, the high fraction of AE ≥ 1 (81%) and histogram peaks above 1.7 indicate a strong dominance of fine-mode aerosols in September, highlighting the widespread biomass burning activity across Africa during this month. In contrast, November is the cleanest month in terms of aerosol load over Africa, with only 18,000 AE quality-assured data over 5 years of AERONET analysis.

We used collocated AERONET and NASA SNPP VIIRS, DB and DT algorithms, AOD data set from 2020 to 2024 to maximize spatial coverage across the continent, including stations established after 2020 in East and South Africa. The collocated pairs were passed through multiple criteria to assure robust sampling in both AERONET and VIIRS. We also ensured that the overall aerosol mode pattern through co-location paired data creation and its criteria is consistent with all the AERONET data analysis, which shows both algorithms capture a fair contribution of seasonality in aerosol modes. DT exhibits more sampling of fine-mode particles in all months. This result is attributed to the higher limitations of DT over bright surfaces, causing its sampling to favor fine particles. September consistently exhibits the highest AE values, median above 1.5, with a narrow and concentrated distribution confirming the dominance of fine-mode aerosols in paired samples. In contrast, April shows the lowest median AE values, below 0.5, indicating a stronger influence of coarse-mode aerosols in the paired data.

The overall comparison of biases exhibits a Gaussian distribution for both DT and DB algorithms. Kernel density estimation (KDE) showed that VIIRS DB shows a slight overestimation with a positive bias of 0.0132 (VIIRS minus AERONET), while DT shows a negative bias of −0.009 (VIIRS minus AERONET), indicating underestimation. While DB shows slightly higher magnitude of bias in the highest frequent peak, the smaller absolute value of the peak in DT could respond to the successful negative shift of the DT bias correction, yet the wider width of bias distribution in DT indicates higher uncertainty in this retrieval algorithm. The distribution analysis is heavily influenced by small AOD values. In the higher-AOD range, linear fits indicate that both algorithms underestimate AOD compared with AERONET. In the scatter plots, DB shows a clear low bias at heavy loading (AOD $>$ 1), while DT exhibits larger scatter and a low-bias trend that appears only in the fitted line as AOD increases. The correlation between VIIRS and AERONET AOD at 550 nm is higher for DB ($\rho = 81\%$) than DT ($\rho = 72\%$). The uncertainty of VIIRS retrieval increases with AOD for both algorithms, with DT exhibiting larger uncertainty (EE = 0.11x + 0.09) compared to DB (EE = 0.07x + 0.07).

We also examined monthly variability in VIIRS uncertainties. These analyses showed that the VIIRS DB algorithm had a higher monthly correlation with AERONET stations, with $\rho > 80\%$ in 4 months, compared to just 1 month for DT. September, August, and October, which also exhibited the highest fraction of the fine-mode aerosols, showed the best EE for the DB algorithm, with September the lowest EE with $0.03\tau_v + 0.06$. May, June, and November exhibited low correlation for both retrieval methods. November is shown to be the cleanest month in terms of AOD contamination, resulting in the lowest number of samples, which potentially also could be reflected in the large EE envelope of $0.30\tau_v + 0.02$ for DB. However, non-homogeneous aerosol modes and types, along with uncertainty in surface reflectance characterization, may also contribute to the observed monthly variability in retrieval uncertainties.

Recent improvements in the fine-mode aerosol model in DB have shown enhanced performance and the lowest correlation coefficient in dominated fine mode, in contrast to dominated coarse mode over land (Lee et al., 2024). As fine particles are generally more dominant in our paired data over Africa, this could explain the better agreement of DB, both in terms of a higher correlation coefficient and a narrower histogram of biases, and smaller EE in contrast to DT. Our monthly analysis further emphasized that September had the lowest EE. Considering that September has the highest number of samples, is the most polluted month in terms of AOD load, and the dominance of fine-mode aerosols during this month further indicates that DB performs particularly well for the retrieval of anthropogenic and smoke aerosols. This also confirms the success of the recently updated in fine mode model of DB.

It is important to note that the data set used in this study is derived from three different retrieval algorithms (DT, and DB from VIIRS and AERONET retrieval algorithm). The differences in performance between the DT and DB algorithms can be attributed to the details of the algorithms such as different surface types, cloud masking, and aerosol property assumptions. As a result, the observed variability may reflect differences in algorithm response to aerosol type and surface conditions combined with their different response to physical aerosol differences. However, the primary objective of this study is to characterize retrieval errors in a manner that supports data assimilation and actionable analysis. Therefore, our emphasis is on the practical error structure of the combined product, rather than on a detailed intercomparison of the underlying algorithm formulations. Using AE as a simple proxy, helps us investigate the potential influence of dominant aerosol modes, for AOD higher than 0.2 to ensure AE quality. The number of samples was more than double for AE $\geq$ 1 compared to AE $<$ 1 for both algorithms. DB performed better in terms of bias, spread around the fit line to AERONET, and EE, in contrast to DT for both AE $\geq$ 1 and AE $<$ 1 grouping.

The Spearman correlation coefficient ($\rho = 0.84$) for AE $<$ 1 indicates strong performance of the VIIRS DB algorithm, despite the AE histogram for this subset showing a mixture of coarse and mixed aerosol modes. A comparable correlation ($\rho = 0.80$) is observed for AE $\geq$ 1 of DB, a subset dominated by fine-mode aerosols as indicated by the AE histogram. AOD ranges were more spread out for AE $<$ 1 up to load of 2 in the paired data, which could possibly influence the higher correlation for AE $<$ 1, in contrast to AE $\geq$ 1, where all paired data were below an AOD load of 1.5. In both AE groupings, DB underestimates large AOD values as AOD increases while overestimating low AOD loads. Our investigations showed that, in terms of bias, DT performs better in AE $\geq$ 1 compared to AE $<$ 1, while the variability of uncertainties showed a consistent large spread and a nonlinear relation with AOD values. The more consistent performance for AE $\geq$ 1 may be related to the more homogeneous

sampling of fine-mode–dominated aerosols in this group, compared with the combination of mixed and coarse aerosols represented by the AE < 1 group.

In addition, the retrieval relies on a limited set of aerosol models representing only a few fine- and coarse-mode types, meaning that mixed aerosol conditions may introduce additional uncertainty and contribute to higher EE in some months. In particular, coarse-mode aerosols are often represented by a single optical model, which may not fully capture the variability of coarse particles. More advanced aerosol modeling in future retrieval algorithms could help reduce uncertainties, particularly for coarse and mixed-mode aerosols. Uncertainty in surface reflectance characterization may further influence the observed monthly variability.

Our findings underscore the importance of regional and seasonal assessment of AOD-retrieval uncertainty, as aerosol sources and characteristics vary by region and month. For data assimilation in air-quality forecasting, monthly uncertainty estimates could inform the observation-error covariance (which is same as EE) and the level of confidence placed in satellite retrievals. Because AOD uncertainties directly influence data assimilation uncertainties, deeper quantification enables realistic expectations about which months will yield better forecast performance. Over Africa, August and September exhibit the lowest uncertainties for the DB product, so AOD assimilation is expected to have the strongest impact in these months. We also show that these months are heavily polluted, with dominant fine-mode aerosols and biomass burning, highlighting DB's potential to improve smoke forecasts during this period over Africa. As both algorithms exhibited underestimation in high AOD loads, while both algorithms show to be able effectively detect anomalous changes and trends, further calibration is needed for enhanced retrieval of heavy load aerosols, which could potentially impact data assimilation and lead to underestimation of high aerosol loads. These high loads often correspond to extreme events that are particularly important to forecast.

In DA system design, product-specific EE definitions can also inform which product to prioritize and how to integrate products when both are available. Over Africa, DB demonstrated better performance; accordingly, when DT and DB are both present, DB could be prioritized, with DT used to extend coverage where DB is missing. Each product should accompany its own covariance-error matrix within the assimilation framework to optimize the use of available data sets while accounting for product-specific limitations.

It should be noted that this study did not analyze the direct impacts of different cloud treatments, land cover, and surface reflectance on the performance of each retrieval algorithm; these factors could be explored in future work to improve cloud treatment and error characterization.

Conflict of Interest

The authors declare no conflicts of interest relevant to this study.

Availability Statement

All data used in this research are publicly available. VIIRS Level-2 data can be downloaded from https://ladsweb.modaps.eosdis.nasa.gov/archive/allData/5201/AERDT_L2_VIIRS_SNPP/ for Dark Target (DT) and https://ladsweb.modaps.eosdis.nasa.gov/search/order/2/AERDB_L2_VIIRS_SNPP--5200 for Deep Blue (DB). AERONET data can be downloaded from https://aeronet.gsfc.nasa.gov/new_web/draw_map_display_inv_v3.html. The pairing code as well as the analyses are available at Bahramvash-Shams (2026).

Acknowledgments
We thank Dr. Manoj Kumar Mishra and the anonymous reviewer for their constructive feedback that helped improve the manuscript. We acknowledge Dr. Hongqing Liu from National Oceanic and Atmospheric Administration for providing the initial pair creation code. This material is based upon work supported by the National Center for Atmospheric Research, which is a major facility sponsored by the National Science Foundation under Cooperative Agreement No. 1852977 as well as NASA SERVIR Grant 80NSSC23K0181.

References

Alexeeff, S. E., Liao, N. S., Liu, X., Eeden, S. K. V. D., & Sidney, S. (2020). Long-term PM2.5 exposure and risks of ischemic heart disease and stroke events: Review and meta-analysis. *Journal of the American Heart Association*, *10*(1), e016890. https://doi.org/10.1161/jaha.120.016890

Bahramvash-Shams, S. (2026). sshamsNCAR/Error_analysis_AOD_NASA_VIIRS_public: April 3, 2026 release (v1.0-review) [Software]. *Zenodo*. https://doi.org/10.5281/zenodo.19411308

Bahramvash-Shams, S., & Mohammadzadeh, A. (2015). A novel aerosol load index using MODIS visible bands: Applied to south-west part of Iran. *IEEE Journal of Selected Topics in Applied Earth Observations and Remote Sensing*, *8*(3), 1167–1175. https://doi.org/10.1109/jstars.2014.2381269

Barkley, A. E., Prospero, J. M., Mahowald, N., Hamilton, D. S., Popendorf, K. J., Oehlert, A. M., et al. (2019). African biomass burning is a substantial source of phosphorus deposition to the Amazon, Tropical Atlantic Ocean, and Southern Ocean. *Proceedings of the National Academy of Sciences*, *116*(33), 16216–16221. https://doi.org/10.1073/pnas.1906091116

Bilal, M., Ali, M. A., Nichol, J. E., Bleiweiss, M. P., de Leeuw, G., Mhawish, A., et al. (2022). AEROsol generic classification using a novel satellite remote sensing Approach (AEROSA). *Frontiers in Environmental Science*, *10*, 981522. https://doi.org/10.3389/fenvs.2022.981522

Boichu, M., Favez, O., Riffault, V., Petit, J.-E., Zhang, Y., Brogniez, C., et al. (2019). Large-scale particulate air pollution and chemical fingerprint of volcanic sulfate aerosols from the 2014–2015 Holuhraun flood lava eruption of Bárðarbunga volcano (Iceland). *Atmospheric Chemistry and Physics*, *19*(22), 14253–14287. https://doi.org/10.5194/acp-19-14253-2019

Boiyo, R., Kumar, K. R., Zhao, T., & Guo, J. (2019). A 10-Year record of aerosol optical properties and radiative forcing over three environmentally distinct AERONET sites in Kenya, East Africa. *Journal of Geophysical Research: Atmospheres*, *124*(3), 1596–1617. https://doi.org/10.1029/2018jd029461

Burnett, R., Chen, H., Szyszkowicz, M., Fann, N., Hubbell, B., Pope, C. A., et al. (2018). Global estimates of mortality associated with long-term exposure to outdoor fine particulate matter. *Proceedings of the National Academy of Sciences*, *115*(38), 9592–9597. https://doi.org/10.1073/pnas.1803222115

Dubovik, O., Holben, B., Eck, T. F., Smirnov, A., Kaufman, Y. J., King, M. D., et al. (2002). Variability of absorption and optical properties of key aerosol types observed in worldwide locations. *Journal of the Atmospheric Sciences*, *59*(3), 590–608. https://doi.org/10.1175/1520-0469(2002)059<0590:voaaop>2.0.co;2

Eck, T. F., Holben, B. N., Reid, J. S., Dubovik, O., Smirnov, A., O'Neill, N. T., et al. (1999). Wavelength dependence of the optical depth of biomass burning, urban, and desert dust aerosols. *Journal of Geophysical Research*, *104*(D24), 31333–31349. https://doi.org/10.1029/1999jd900923

Eck, T. F., Holben, B. N., Sinyuk, A., Pinker, R. T., Goloub, P., Chen, H., et al. (2010). Climatological aspects of the optical properties of fine/coarse mode aerosol mixtures. *Journal of Geophysical Research*, *115*(D19). https://doi.org/10.1029/2010jd014002

Ettehadi Osgouei, P. E., Roberts, G., Kaya, S., Bilal, M., Dash, J., & Sertel, E. (2022). Evaluation and comparison of MODIS and VIIRS aerosol optical depth (AOD) products over regions in the Eastern Mediterranean and the Black Sea. *Atmospheric Environment*, *268*, 118784. https://doi.org/10.1016/j.atmosenv.2021.118784

Giles, D. M., Holben, B. N., Eck, T. F., Sinyuk, A., Smirnov, A., Slutsker, I., et al. (2012). An analysis of AERONET aerosol absorption properties and classifications representative of aerosol source regions. *Journal of Geophysical Research*, *117*(D17). https://doi.org/10.1029/2012jd018127

Giles, D. M., Sinyuk, A., Sorokin, M. G., Schafer, J. S., Smirnov, A., Slutsker, I., et al. (2019). Advancements in the Aerosol Robotic Network (AERONET) version 3 database—Automated near-real-time quality control algorithm with improved cloud screening for Sun photometer aerosol optical depth (AOD) measurements. *Atmospheric Measurement Techniques*, *12*(1), 169–209. https://doi.org/10.5194/amt-12-169-2019

Ginoux, P., Prospero, J. M., Gill, T. E., Hsu, N. C., & Zhao, M. (2012). Global-scale attribution of anthropogenic and natural dust sources and their emission rates based on MODIS Deep Blue aerosol products. *Reviews of Geophysics*, *50*(3). https://doi.org/10.1029/2012rg000388

Ginoux, P., Prospero, J. M., Torres, O., & Chin, M. (2004). Long-term simulation of global dust distribution with the GOCART model: Correlation with North Atlantic Oscillation. *Environmental Modelling and Software*, *19*(2), 113–128. https://doi.org/10.1016/s1364-8152(03)00114-2

Hart, N. C. G., Reason, C. J. C., & Fauchereau, N. (2013). Cloud bands over southern Africa: Seasonality, contribution to rainfall variability and modulation by the MJO. *Climate Dynamics*, *41*(5–6), 1199–1212. https://doi.org/10.1007/s00382-012-1589-4

Hill, A. E., Hühner, T., Kreibich, V., & Lindner, C. (2014). Dar es Salaam, megacity of tomorrow: Informal urban expansion and the provision of technical infrastructure. In *Dar es Salaam, megacity of tomorrow*. https://doi.org/10.1007/978-90-481-3417-5_12

Holben, B. N., Eck, T. F., Slutsker, I., Tanré, D., Buis, J. P., Setzer, A., et al. (1998). AERONET—A federated instrument network and data archive for aerosol characterization. *Remote Sensing of Environment*, *66*(1), 1–16. https://doi.org/10.1016/s0034-4257(98)00031-5

Hsu, N. C., Jeong, M.-J., Bettenhausen, C., Sayer, A. M., Hansell, R., Seftor, C. S., et al. (2013). Enhanced Deep Blue aerosol retrieval algorithm: The second generation. *Journal of Geophysical Research: Atmospheres*, *118*(16), 9296–9315. https://doi.org/10.1002/jgrd.50712

Hsu, N. C., Lee, J., Sayer, A. M., Kim, W., Bettenhausen, C., & Tsay, S.-C. (2019). VIIRS deep blue aerosol products over land: Extending the EOS long-term aerosol data records. *Journal of Geophysical Research: Atmospheres*, *124*(7), 4026–4053. https://doi.org/10.1029/2018jd029688

Huang, B., Pagowski, M., Trahan, S., Martin, C. R., Tangborn, A., Kondragunta, S., & Kleist, D. T. (2023). JEDI-Based three-dimensional ensemble-variational data assimilation system for global aerosol forecasting at NCEP. *Journal of Advances in Modeling Earth Systems*, *15*(4), e2022MS003232. https://doi.org/10.1029/2022ms003232

Huang, J., Kondragunta, S., Laszlo, I., Liu, H., Remer, L. A., Zhang, H., et al. (2016). Validation and expected error estimation of Suomi-NPP VIIRS aerosol optical thickness and Ångström exponent with AERONET. *Journal of Geophysical Research: Atmospheres*, *121*(12), 7139–7160. https://doi.org/10.1002/2016jd024834

Ichoku, C., & Ellison, L. (2014). Global top-down smoke-aerosol emissions estimation using satellite fire radiative power measurements. *Atmospheric Chemistry and Physics*, *14*(13), 6643–6667. https://doi.org/10.5194/acp-14-6643-2014

Jackson, J. M., Liu, H., Laszlo, I., Kondragunta, S., Remer, L. A., Huang, J., & Huang, H. (2013). Suomi-NPP VIIRS aerosol algorithms and data products. *Journal of Geophysical Research: Atmospheres*, *118*(22), 12673–12689. https://doi.org/10.1002/2013jd020449

Kabir, F., Yu, N., Yao, W., Wu, L., Jiang, J. H., Gu, Y., & Su, H. (2018). Impact of aerosols on reservoir inflow: A case study for Big Creek Hydroelectric System in California. *Hydrological Processes*, *32*(22), 3365–3390. https://doi.org/10.1002/hyp.13265

Kahn, R. A., Gaitley, B. J., Garay, M. J., Diner, D. J., Eck, T. F., Smirnov, A., & Holben, B. N. (2010). Multiangle Imaging SpectroRadiometer global aerosol product assessment by comparison with the Aerosol Robotic Network. *Journal of Geophysical Research*, *115*(D23). https://doi.org/10.1029/2010jd014601

Kaufman, Y. J., Tanré, D., Remer, L. A., Vermote, E. F., Chu, A., & Holben, B. N. (1997). Operational remote sensing of tropospheric aerosol over land from EOS moderate resolution imaging spectroradiometer. *Journal of Geophysical Research*, *102*(D14), 17051–17067. https://doi.org/10.1029/96jd03988

Kleinman, L. I., Sedlacek III, A. J., Adachi, K., Buseck, P. R., Collier, S., Dubey, M. K., et al. (2020). Rapid evolution of aerosol particles and their optical properties downwind of wildfires in the western US. *Atmospheric Chemistry and Physics*, *20*(21), 13319–13341. https://doi.org/10.5194/acp-20-13319-2020

Koren, I., Altaratz, O., Remer, L. A., Feingold, G., Martins, J. V., & Heiblum, R. H. (2012). Aerosol-induced intensification of rain from the tropics to the mid-latitudes. *Nature Geoscience*, *5*(2), 118–122. https://doi.org/10.1038/ngeo1364

Kumar, R., Ghude, S. D., Biswas, M., Jena, C., Alessandrini, S., Debnath, S., et al. (2020). Enhancing accuracy of air quality and temperature forecasts during paddy crop residue burning season in Delhi via chemical data assimilation. *Journal of Geophysical Research: Atmospheres*, *125*(17), e2020JD033019. https://doi.org/10.1029/2020jd033019

Lee, J., Hsu, N. C., Kim, W. V., Sayer, A. M., & Tsay, S. (2024). VIIRS version 2 deep blue aerosol products. *Journal of Geophysical Research: Atmospheres*, *129*(6), e2023JD040082. https://doi.org/10.1029/2023jd040082

Levy, R. C., Mattoo, S., Munchak, L. A., Remer, L. A., Sayer, A. M., Patadia, F., & Hsu, N. C. (2013). The Collection 6 MODIS aerosol products over land and ocean. *Atmospheric Measurement Techniques*, *6*(11), 2989–3034. https://doi.org/10.5194/amt-6-2989-2013

Levy, R. C., Mattoo, S., Sawyer, V., Kiliyanpilakkil, P., Shi, Y., Gupta, P., et al. (2024). *Algorithm for remote sensing of tropospheric aerosol over dark targets: Algorithm Theoretical Basis Document (ATBD)*. NASA Goddard Space Flight Center. Retrieved from https://darktarget.gsfc.nasa.gov/sites/default/files/users/user9/ATBD_DarkTarget_April3.pdf

Levy, R. C., Mattoo, S., Sawyer, V., Shi, Y., Colarco, P. R., Lyapustin, A. I., et al. (2018). Exploring systematic offsets between aerosol products from the two MODIS sensors. *Atmospheric Measurement Techniques*, *11*(7), 4073–4092. https://doi.org/10.5194/amt-11-4073-2018

Levy, R. C., Remer, L. A., & Dubovik, O. (2007). Global aerosol optical properties and application to Moderate Resolution Imaging Spectroradiometer aerosol retrieval over land. *Journal of Geophysical Research*, *112*(D13), D13210. https://doi.org/10.1029/2006JD007815

Liu, H., Remer, L. A., Huang, J., Huang, H., Kondragunta, S., Laszlo, I., et al. (2014). Preliminary evaluation of S-NPP VIIRS aerosol optical thickness. *Journal of Geophysical Research: Atmospheres*, *119*(7), 3942–3962. https://doi.org/10.1002/2013jd020360

Liu, Y., Hua, S., Jia, R., & Huang, J. (2019). Effect of aerosols on the ice cloud properties over the Tibetan Plateau. *Journal of Geophysical Research: Atmospheres*, *124*(16), 9594–9608. https://doi.org/10.1029/2019jd030463

Liu, Z., Liu, Q., Lin, H., Schwartz, C. S., Lee, Y., & Wang, T. (2011). Three-dimensional variational assimilation of MODIS aerosol optical depth: Implementation and application to a dust storm over East Asia. *Journal of Geophysical Research*, *116*(D23). https://doi.org/10.1029/2011jd016159

Martins, V. S., Lyapustin, A., de Carvalho, L. A. S., Barbosa, C. C. F., & Novo, E. M. L. M. (2017). Validation of high-resolution MAIAC aerosol product over South America. *Journal of Geophysical Research: Atmospheres*, *122*(14), 7537–7559. https://doi.org/10.1002/2016jd026301

Meng, F., Cao, C., & Shao, X. (2015). Spatio-temporal variability of Suomi-NPP VIIRS-derived aerosol optical thickness over China in 2013. *Remote Sensing of Environment*, *163*, 61–69. https://doi.org/10.1016/j.rse.2015.03.005

Mishra, M. K., Misra, A., & Kumar, R. (2023). Operational AOD retrieval at subkilometer resolution using OceanSat-2 OCM over land: SAER Algorithm, uncertainties, Validation and Inter-Sensor Comparison. *Earth and Space Science*, *10*(7), e2023EA002896. https://doi.org/10.1029/2023ea002896

Mishra, M. K., Shameela, S. F., Rathore, P. S., et al. (2025). Advancing global aerosol classification: Source-compositional typology and variability from 30 years (1993–2024) of AERONET observations. *Science of the Total Environment*, *890*, 180301. https://doi.org/10.1016/j.scitotenv.2025.180301

Morcrette, J.-J., Boucher, O., Jones, L., Salmond, D., Bechtold, P., Beljaars, A., et al. (2009). Aerosol analysis and forecast in the European Centre for Medium-Range Weather Forecasts Integrated Forecast System: Forward modeling. *Journal of Geophysical Research*, *114*(D6). https://doi.org/10.1029/2008jd011235

NASA-Aqua. (2025). Aqua earth-observing satellite Mission. Retrieved from https://aqua.nasa.gov/

NASA-Terra. (2025). Terra orbit infomation. Retrieved from https://terra.nasa.gov/

Payra, S., Sharma, A., Mishra, M. K., & Verma, S. (2023). Performance evaluation of MODIS and VIIRS satellite AOD products over the Indian subcontinent. *Frontiers in Environmental Science*, *11*, 1158641. https://doi.org/10.3389/fenvs.2023.1158641

Pei, X., Yang, L., Ji, W., Li, M., Peng, Z., Cheng, X., & Lu, X. (2025). Global evaluation of NOAA-20 VIIRS dark target aerosol products over land and ocean. *Atmospheric Environment*, *342*, 120949. https://doi.org/10.1016/j.atmosenv.2024.120949

Petrenko, M., Ichoku, C., & Leptoukh, G. (2012). Multi-sensor Aerosol Products Sampling System (MAPSS). *Atmospheric Measurement Techniques*, *5*(5), 913–926. https://doi.org/10.5194/amt-5-913-2012

Ramanathan, V., Crutzen, P. J., Kiehl, J. T., & Rosenfeld, D. (2001). Aerosols, climate, and the hydrological cycle. *Science*, *294*(5549), 2119–2124. https://doi.org/10.1126/science.1064034

Remer, L. A., Kaufman, Y. J., Tanré, D., Mattoo, S., Chu, D. A., Martins, J. V., et al. (2005). The MODIS aerosol Algorithm, products, and validation. *Journal of the Atmospheric Sciences*, *62*(4), 947–973. https://doi.org/10.1175/jas3385.1

Ridley, D. A., Heald, C. L., & Ford, B. (2012). North African dust export and deposition: A satellite and model perspective. *Journal of Geophysical Research*, *117*(D2). https://doi.org/10.1029/2011jd016794

Roberts, G., Wooster, M. J., & Lagoudakis, E. (2009). Annual and diurnal African biomass burning temporal dynamics. *Biogeosciences*, *6*(5), 849–866. https://doi.org/10.5194/bg-6-849-2009

Rosenfeld, D., Andreae, M. O., Asmi, A., Chin, M., de Leeuw, G., Donovan, D. P., et al. (2014). Global observations of aerosol-cloud-precipitation-climate interactions. *Reviews of Geophysics*, *52*(4), 750–808. https://doi.org/10.1002/2013rg000441

Sawyer, V., Levy, R. C., Mattoo, S., Shi, Y. R., Kim, M., Remer, L. A., & Cureton, G. (2025). An updated VIIRS dark target aerosol product for continuity with MODIS: Assessing regional aerosol trends. *Frontiers in Environmental Science*, *13*, 1602145. https://doi.org/10.3389/fenvs.2025.1602145

Sawyer, V., Levy, R. C., Mattoo, S., Cureton, G., Shi, Y., & Remer, L. A. (2020). Continuing the MODIS dark target aerosol time series with VIIRS. *Remote Sensing*, *12*(2), 308. https://doi.org/10.3390/rs12020308

Sayer, A. M. (2020). How long is too long? Variogram analysis of AERONET data to aid aerosol validation and intercomparison studies. *Earth and Space Science*, *7*(9), e2020EA001290. https://doi.org/10.1029/2020ea001290

Schumacher, V., & Setzer, A. (2024). Assessment and characteristics of S-NPP VIIRS Deep Blue and Dark Target aerosol properties under clean, polluted and fire scenarios over the Amazon. *Atmospheric Environment*, *323*, 120398. https://doi.org/10.1016/j.atmosenv.2024.120398

Schuster, G. L., Dubovik, O., & Holben, B. N. (2006). Angstrom exponent and bimodal aerosol size distributions. *Journal of Geophysical Research*, *111*(D7). https://doi.org/10.1029/2005jd006328

Shi, Y., Zhang, J., Reid, J. S., Hyer, E. J., & Hsu, N. C. (2013). Critical evaluation of the MODIS Deep Blue aerosol optical depth product for data assimilation over North Africa. *Atmospheric Measurement Techniques*, *6*(4), 949–969. https://doi.org/10.5194/amt-6-949-2013

Streets, D. G., Bond, T. C., Carmichael, G. R., Fernandes, S. D., Fu, Q., He, D., et al. (2003). An inventory of gaseous and primary aerosol emissions in Asia in the year 2000. *Journal of Geophysical Research*, *108*(D21). https://doi.org/10.1029/2002jd003093

Tatro, T., & Zuidema, P. (2025). More biomass burning aerosol is being advected westward over the southern tropical Atlantic since 2003. *Science of the Total Environment*, *965*, 178506. https://doi.org/10.1016/j.scitotenv.2025.178506

van der Werf, G. R., Randerson, J. T., Giglio, L., van Leeuwen, T. T., Chen, Y., Rogers, B. M., et al. (2017). Global fire emissions estimates during 1997–2016. *Earth System Science Data*, *9*(2), 697–720. https://doi.org/10.5194/essd-9-697-2017

Xu, R., Ye, T., Yue, X., Yang, Z., Yu, W., Zhang, Y., et al. (2023). Global population exposure to landscape fire air pollution from 2000 to 2019. *Nature*, *621*(7979), 521–529. https://doi.org/10.1038/s41586-023-06398-6

Yu, H., Chin, M., Yuan, T., Bian, H., Remer, L. A., Prospero, J. M., et al. (2015). The fertilizing role of African dust in the Amazon rainforest: A first multiyear assessment based on data from Cloud-Aerosol LiDAR and Infrared Pathfinder Satellite Observations. *Geophysical Research Letters*, *42*(6), 1984–1991. https://doi.org/10.1002/2015gl063040

Yu, H., Remer, L. A., Kahn, R. A., Chin, M., & Zhang, Y. (2013). Satellite perspective of aerosol intercontinental transport: From qualitative tracking to quantitative characterization. *Atmospheric Research*, *124*, 73–100. https://doi.org/10.1016/j.atmosres.2012.12.013

Zhang, Z., Li, J., Che, H., Dong, Y., Dubovik, O., Eck, T., et al. (2025). Long-term trends in aerosol properties derived from AERONET measurements. *Atmospheric Chemistry and Physics*, *25*(8), 4617–4637. https://doi.org/10.5194/acp-25-4617-2025

Zhu, J., Xia, X., Wang, J., Che, H., Chen, H., Zhang, J., et al. (2017). Evaluation of aerosol optical depth and aerosol models from VIIRS retrieval algorithms over North China Plain. *Remote Sensing*, *9*(5), 432. https://doi.org/10.3390/rs9050432